STMN2 protein depletion via translation deficits and stress granules in amyotrophic lateral sclerosis

ELLIS, Brittany C S, AVILA, Anna Sanchez, HUANG, Wan-Ping, JOHN, Sabin J, BONSALL, Sam, HODGSON, Rachel E, KUMAR, Vedanth, NOLAN, Matthew, WEST, Ryan J H <http://orcid.org/0000-0001-9873-2258>, CAMPBELL, Susan <http://orcid.org/0000-0002-6740-1445>, DE VOS, Kurt J <http://orcid.org/0000-0003-2161-6309>, LAGIER-TOURENNE, Clotilde, ROBIN HIGHLEY, J, COOPER-KNOCK, Johnathan <http://orcid.org/0000-0002-0873-8689> and SHELKOVNIKOVA, Tatyana A <http://orcid.org/0000-0003-1367-5309>

STMN2 protein depletion via translation deficits and stress granules in amyotrophic lateral sclerosis

Brittany C. S. Ellis,[1] Anna Sanchez Avila,[1] Wan-Ping Huang,[1] Sabin J. John,[1] Sam Bonsall,[1] Rachel E. Hodgson,[1] Vedanth Kumar,[1] Matthew Nolan,[2] Ryan J. H. West,[1] Susan G. Campbell,[3] Kurt J. De Vos,[1] Clotilde Lagier-Tourenne,[2] J. Robin Highley,[1] Johnathan Cooper-Knock[1] and Tatyana A. Shelkovnikova[1]

Abstract

STMN2 is an abundant neurospecific protein dysregulated in neurodegenerative diseases such as amyotrophic lateral sclerosis (ALS). We previously reported that cellular stress can lead to STMN2 loss due to TDP-43 nuclear condensation. Here, using human and murine neuronal cell models, multiple pharmacological tools, *in situ* single-molecule analysis of translation and RNA localisation, and longitudinal analysis of neuronal fitness/survival, we establish TDP-43-independent mechanisms of STMN2 depletion under stress.

We find that human STMN2 protein level is extremely labile under acute high-magnitude stress. Early in stress, STMN2 is suppressed via activated proteasomal degradation, phosphorylation and translation repression by stress granules, independently of TDP-43 loss of function in splicing. We further show that STMN2 protein level is highly sensitive to chronic translation deficits, such as those elicited by prolonged low-grade stress. We find that low pre-stress STMN2 sensitises neuronal cells to stress-induced apoptosis, whereas moderately increased STMN2 is protective under stress. Finally, we demonstrate that STMN2 mRNA is upregulated in non-TDP ALS (ALS-FUS) models, which may compensate for translation/stress granule defects in this disease subtype. Consistent with the compensation hypothesis, STMN2 mRNA is also upregulated in the relatively spared (cortex), but not severely affected (spinal cord), CNS regions in ALS-TDP.

In conclusion, our study implicates two common denominators in neurodegeneration – dysregulation of translation and stress granules – in STMN2 depletion, independent of TDP-43 loss of function. It also describes an RNA-based compensatory mechanism in ALS underling the unique vulnerability of neurons with developing TDP-43 pathology.

Author affiliations:

1 Sheffield Institute for Translational Neuroscience (SITraN) and Neuroscience Institute, University of Sheffield, Sheffield, S10 2HQ, UK

2 Department of Neurology, The Sean M. Healey and AMG Center for ALS at Mass General, Massachusetts General Hospital, Harvard Medical School, Boston, MA 02114, USA

3 Biomolecular Sciences Research Centre, School of Biosciences and Chemistry, Sheffield Hallam University, Sheffield, S1 1WB, UK

Correspondence to: Tatyana Shelkovnikova

SITraN, 385 Glossop Road, Sheffield S10 2HQ, UK

E-mail: t.shelkovnikova@sheffield.ac.uk

Running title: TDP-43-independent STMN2 loss mechanisms

Keywords: ALS; STMN2; TDP-43; stress granule; protein translation; FUS

Introduction

STMN2, a neurospecific protein, has recently emerged as a molecular factor dysregulated in neurodegenerative conditions with TDP-43 proteinopathy, including subsets of amyotrophic lateral sclerosis (ALS), frontotemporal dementia (FTD), and Alzheimer's disease[1-3]. Mechanistically, STMN2 pre-mRNA has TDP-43 binding sites in the vicinity of a cryptic exon (CE; exon 2a) in intron 1, and this CE is preferentially spliced in upon TDP-43 dysregulation. This results in STMN2 mRNA truncation, ultimately leading to reduced STMN2 protein synthesis[4]. STMN2 has also been implicated in ALS with SOD1 mutations, spinal muscular atrophy[5] and Parkinson's disease[6]. Stmn2 knockout causes neuropathy in mice[7-9]. Thus, loss of STMN2 homeostasis may act as a convergent pathway of neuronal degeneration across several neurological diseases.

STMN2 (aka SCG10) is a conserved phosphoprotein[10] expressed from one of the 25 most abundant mRNAs in human and rodent motor neurons[11]. It has an important role in neurite outgrowth, being highly expressed in the developing neurons[12], and is recruited to the

growth cones of regenerating axons after axonal injury[13]. STMN2 inhibits microtubule polymerisation and therefore regulates the dynamism of this process – required for both neurite growth in the development and axonal regeneration in the adult state[14].

We have recently demonstrated that acute cellular stress, such as short exposure to arsenite, results in rapid and profound STMN2 downregulation, correlating with TDP-43 nuclear condensation and its loss of solubility[15]. Importantly, although stress-induced changes in TDP-43-regulated splicing impact multiple TDP-43 targets, STMN2 is particularly sensitive[15]. Stress may play an important role in neurodegenerative diseases that have a multifactorial nature and 4-6 discrete steps in their pathogenesis[16, 17]. For example, experimental evidence points to a role for vigorous exercise leading to the build-up of reactive oxygen species[18], viral infections[19-21] and stress-induced proteostasis impairment[22], although the exact nature of extrinsic factors that act as "second hits" in ALS is yet to be elucidated. Better understanding of STMN2 regulation under stress may provide novel clues into the pathogenesis of ALS and other TDP-43 proteinopathies.

Here we report that STMN2 protein is disproportionately affected by stress response, both acute and chronic. Acute stress causes its rapid depletion due to activated proteasome degradation and stress granule-mediated translation repression, preceding cryptic splicing-mediated depletion due to TDP-43 loss-of-function. On the other hand, being an extremely short-lived protein, STMN2 is highly sensitive to mild impairment of protein synthesis such as that associated with chronic low-grade stress. Analysis of human post-mortem tissue revealed that STMN2 protein level is maintained in non-TDP ALS (FUS and SOD1) – despite reported translation deficits and/or stress granule misregulation in these subtypes. Data from cell models suggested compensatory STMN2 mRNA upregulation as a possible mechanism. Consistent with the ongoing compensation at the RNA level, STMN2 mRNA is also upregulated in the relatively spared CNS areas in ALS-TDP.

Thus, we report novel molecular insights into STMN2 regulation under stress and in neurodegeneration, linking this protein to the hallmarks of neurodegenerative diseases – misregulation of protein translation and stress granule metabolism.

Materials and methods

General cell culture, plasmids, transfection and transduction

Human SH-SY5Y neuroblastoma cells were obtained from ATCC via Sigma and cultured in DMEM/F-12 supplemented with 10% FBS and penicillin-streptomycin (all Thermo Fisher

Scientific). Neuro2a (N2a) murine cells (ATCC lines, gift of G.Hautbergue) were cultured in DMEM/F-12 supplemented with 2 mM Glutamine, 1% Non-Essential Amino Acids (NEAA), 1 mM sodium pyruvate, and 10% FBS. Plasmids for the expression of GFP-tagged G3BP1, GFP-tagged STMN2 WT/3A and V5-tagged STMN2 (all in pEGFP-N1 vector) and were custom-made by Genewiz and verified by sequencing. STMN2 siRNA was from ThermoFisher (SilencerSelect®) and scrambled control siRNA was AllStars from Qiagen. Cells were transfected using Lipofectamine2000. Plasmids and lentiviral particles for the expression of untagged STMN2 and Cry2olig (used as control) were prepared as described in our previous study[23]. Cells were transduced with an MOI of 2 (low titre) or 10 (high titre) by directly adding lentiviral particles to the culturing media.

Motor neuron differentiation

Human motor neurons were differentiated from the KOLF2.1J iPSC line (obtained from iNDI/JAX, JIPSC001000) as described for human ES cells previously[24], with modifications. Briefly, iPSCs were maintained on Matrigel® (Corning)-coated 6-well plates in mTeSR Plus (Stemcell Technologies), with media changes daily. At 90% confluency, cells were detached using ReLeSR® (Stemcell Technologies) and re-plated at 1:4 ratio using Rock kinase inhibitor Y-27632 (ApexBio), with a complete media change after 24 hours. At 70-80% confluency, media was changed to "DM1" differentiation medium composed of Advanced DMEM/F12 (ADF) with 10 µM SB431542 (Abcam) and B27 supplement (without vitamin A; Gibco). Daily media changes were performed throughout differentiation with supplements added according to the differentiation stage. On day 4, purmorphamine (1 µM, Cayman Chemicals) and retinoic acid (0.1 µM, Sigma) were added to DM1 and cells were cultured in this medium ("DM2") until day 16. Neural precursors (NPCs) were split at 1:2 ratio on day 8 and on day 16 using Accutase®. From day 16, NPCs were transferred to "DM3" medium composed of ADF, B27 and 1 µg/ml human BDNF (Miltenyi). On day 23, motor neurons were split at 1:2 ratio using Accutase and re-plated in DM3 media. After recovery, the cells were changed into "DM4" media – DM3 with half of ADF replaced with Neurobasal A (Gibco) and N2 supplement (Gibco), and matured for 7 days, before re-plating in the final (experimental) format.

Chemical treatments

Pharmacological treatments (Merck/Sigma unless indicated otherwise): $NaAsO_2$ (concentrations indicated in Results/figure legends), MG132 (10 µM), chloroquine (100 µM), thapsigargin (10 µM), poly(I:C) (100 ng per well), ISRIB (1 µM), lipoamide (10 µM), silvestrol (100 nM), rocaglamide A (100 nM), sorbitol (0.45 M), thapsigargin (10 µM), cycloheximide (10 µg/ml), pitavastatin and simvastatin (both ApexBio; concentrations indicated in the Results/figure legends). Incubation times and other modifications to the

protocol are indicated in the respective Figure legend and Results section. Me4BodipyFL-Ahx3Leu3VS (Proteasome Activity Probe, I-190, R&D Systems) was added to live cells (10 μM final concentration) 5 min prior to imaging on Opera Phenix.

Immunocytochemistry, puro-PLA and fluorescent microscopy

Immunocytochemistry was performed on cells growing either on 10-mm coverslips (VWR) in 24-well plates or on cells growing in 96-well optical plates. Cells were fixed with 4% PFA in 1xPBS, washed with 1xPBS and kept in 70% ethanol at 4°C. Immunostaining was performed as described earlier[25] using commercially available antibodies (1:1000 dilution): STMN2 (rabbit polyclonal, Proteintech, 10586-1-AP or mouse monoclonal, Proteintech, 67204-1-Ig); TDP-43 (rabbit polyclonal, C-terminal, Sigma, T1580, or mouse monoclonal, R&D Systems, MAB7778); G3BP1 (rabbit polyclonal, Proteintech, 13057-2-AP); GM130 (rabbit polyclonal, Proteintech, 11308-1-AP); Tuj/betaIII-tubulin (rabbit recombinant monoclonal Alexa488-labelled, Abcam, AB237350); STMN3 (rabbit polyclonal, Proteintech 11311-1-AP); OPTN (rabbit polyclonal, Proteintech, 10837-1-AP); HuR/ELAVL1 (rabbit polyclonal, Proteintech, 11910-1-AP); MATR3 (rabbit polyclonal, Proteintech, 12202-2-AP). For puromycin labelling coupled with proximity ligation assay (puro-PLA), cells were cultured in optical plates. Puromycin (Sigma, 1 μg/ml) was added directly to media for the indicated time, cells were fixed as above and incubated in a combination of primary antibodies (1:1000) against puromycin (mouse monoclonal, Merck, MABE343) and STMN2 (rabbit polyclonal, Proteintech) diluted in PBST, overnight at 4°C. PLA was performed using Duolink® In Situ Orange Starter Kit Mouse/Rabbit (Merck/Sigma). Nuclei were stained with DAPI. Conventional fluorescence microscopy of immunostained cells was performed using a 100x oil objective on an Olympus BX57 upright microscope equipped with ORCA-Flash 4.0 camera (Hamamatsu) and cellSens Dimension software (Olympus). High-content microscopy in the 96-well format was performed on Opera Phenix and Harmony 4.9 software.

RNA *in situ* hybridization

RNA-FISH was performed using a custom STMN2 mRNA probe set (24 probes, Supplementary Table 1) designed and synthesised by Biosearch Technologies as described[25]. BaseScopeISH was performed with the probes for full-length STMN2 mRNA – 1048241-C1 (exon one) or 1048231-C1 (exons four and five) (ACDBio) – according to the manufacturer's instructions. Briefly, cells grown on coverslips were fixed with 10% neutral buffered formalin for 30 min at RT on a flat-surface shaker. Cells were then gradually dehydrated in ethanol with ascending concentration for 5 min each and kept in 100% ethanol at -20°C. Coverslips were rehydrated by ethanol washes with descending concentration for 5 min each, before 1xPBS was added to coverslips for 10 min. Samples

were then treated with 30 µl protease III (ACDBio) at RT for 15 min. Coverslips were washed with fresh 1xPBS, before incubating in 30 µl of a BaseScope probe for two hours at 40°C in HybEZ oven. Signal was detected using BaseScope Detection kit (ACDBio), according to manufacturer instructions, after which Fast Red substrate was added for 10 min at RT. Coverslips were mounted onto glass slides with Immu-Mount (ThermoFisher).

Image analysis and quantification

Quantification of RNA-FISH experiments was performed using custom pipelines on Image J. Automated quantification of stress granules was carried out using a custom pipeline (Spot analysis) on Harmony 4.9 software as described[26]. Automated quantification of puro-PLA signals was performed using a custom Spot analysis pipeline on Harmony 4.9. For the analysis with the proteasome activity probe, fluorescence intensity (GFP channel) was measured in individual cells using Harmony 4.9 software.

Longitudinal analysis of cell viability on Incucyte

SH-SY5Y cells and Day 32 human motor neurons were plated onto optical 96-well plates (Phenoplate-96). Motor neurons were matured directly on plates for 7 days before the analysis. Viability and proliferation analysis was performed on Incucyte® S3 Live-Cell Analysis System (Sartorius), by recording cell density in the bright-field (Phase Object Count) and apoptosis rate with the Incucyte® Caspase-3/7 Green Dye (Green Object Count).

RNA expression analysis

Total RNA was extracted using GenElute total mammalian RNA kit (Sigma) or QiaZOL (Qiagen) in accordance with the manufacturer's instructions. First-strand cDNA synthesis was performed using 500 ng of RNA with random primers (ThermoFisher) and MMLV reverse transcriptase (Promega). qRT-PCR was performed using qPCRBIO SyGreen Lo-ROX (PCRbio), and GAPDH was used for normalisation. Human-specific primers from a previous study were used[15], and STMN2 pre-mRNA primers were as follows: 5'-CTCGGCAGAAGACCTTCGAG-3' and 5'-ACAAGCCGCATTCACATTCA-3'. Mouse-specific primers were as follows: Stmn2, 5'-CTCCTCATGGATTACGCGCT-3' and 5'-TCAGCACGTTGGAAGGTTCA-3'; Gapdh, 5'-AGGTCGGTGTGAACGGATTTG-3' and 5'-GGGGTCGTTGATGGCAACA-3'.

In vitro protein assays

For the analysis of STMN2 phosphorylation, cells were lysed in the lysis buffer (50 mM Tris HCl, 150 mM NaCl, 1% Triton-X100, protease inhibitor cocktail), scraped, and suspension was vortexed every 5 min for 30 min for complete cell lysis. Lysate was mixed with 2x Calf

Intestinal Alkaline Phosphatase (CIP) in reaction buffer (50mM NaCl, 50mM Tris-HCl, 20mM $MgCl_2$, 2mM DTT, protease inhibitor cocktail), based on 1 unit per 1 µg protein (or the same volume of water as control). Samples were incubated with CIP at 37°C for 1 hour and analysed by western blot. For the analysis of STMN2 solubility under stress, samples were incubated in the urea lysis buffer – 50mM Tris, 150mM NaCl, 0.5% Triton-X, 8M urea, before mixing with 2xLaemmli buffer and proceeding to western blot. For puromycilation (measurement of protein translation rates), cells were pulsed with puromycin for 10 min prior to lysis.

Western blotting

Cells were lysed in 2xLaemmli buffer, and the samples were heated at 95°C for 15 min. Samples were resolved on a 10% Mini-PROTEAN® TGX™ hand-cast protein gel (Bio-Rad) and transferred to a PVDF membrane (Amersham). Gels were stained with Gelcode™ (ThermoFisher) post-transfer for total protein (loading control). Membranes were blocked for one hour in 4% non-fat milk/TBST and then incubated with primary antibodies (1:500 for puromycin and 1:1000 all others) at 4°C overnight: STMN2 (rabbit polyclonal, Proteintech, 10586-1-AP); TDP-43 (rabbit polyclonal, C-terminal, Sigma); p-eIF2α (rabbit monoclonal, Abcam, ab32157); total eIF2α (rabbit polyclonal, Cell Signaling, 9722), and puromycin (mouse monoclonal, Merck, MABE343). Anti-rabbit or anti-mouse HRP secondary antibody (GE Healthcare/Amersham) incubation was performed for one hour at RT in 4 % milk/TBST. Signal was detected using Clarity Max Western ECL Substrate (Bio-Rad) and quantified using Licor Odyssey FC/Image Studio software or Image J.

Analysis in human tissue

Spinal cord sections from neuropathologically characterised individuals from the Sheffield Brain Tissue Bank (SBTB) were used (see Supplementary Table 2). SBTB has ethical permission to function as a research tissue bank from the Wales Research Ethics Committee 5 (Reference 24/WA/0052). SBTB adheres to consenting protocols laid down by the UK Human Tissue Authority and agreed to by the Research Ethics Committee. Diagnosis in all cases was confirmed by qualified neuropathologist, neurologist and clinical geneticist working in UKAS- and CQC-accredited facilities. Sections (7 µm-thick) were processed for immunohistochemistry as described before[27], except antigen retrieval in 10 mM sodium citrate (pH 6.0) was performed in a pressure cooker and TBS buffer was used for the washes. Sections were immunostained for STMN2 using a rabbit polyclonal antibody (Proteintech, 10586-1-AP; 1:1000), mouse monoclonal antibody (Proteintech, 67201-1-Ig; 1:1000) or mouse monoclonal phospho-TDP-43 antibody (Ser409/410, CosmoBio, TIP-PTD-M01A; 1:8000) with ImPACT® DAB reagent kit used for signal detection. BaseScopeISH analysis on rehydrated sections was performed as described

above for cells on coverslips; 1048231-C1 probe was used. Imaging was done either on Hamamatsu NanoZoomer XR slide scanner or on Nikon Eclipse microscope. Image analysis (pixel intensity) was performed using QuPath v0.5.1 software. qRT-PCR analysis on homogenised motor cortex samples was performed as described above for cultured cells.

Analysis of the RNA-seq datasets from the NYGC ALS consortium

The NYGC cohort RNA sequencing data was obtained from GEO omnibus (GEO accession no. GSE137810). Raw counts were converted to approximate RPKM values using gene length estimations and per-sample library size scaling. Counts corresponding to STMN2 mRNA were identified by filtering for Ensembl gene identifier ENSG00000104435. ALS samples were then classified as TDP-related ALS, ALS-SOD1 and ALS-FUS based on the "Subject Group" metadata field, and TPM for STMN2 plotted individually for motor cortex, frontal cortex and spinal cord tissues. Statistical comparisons between ALS and control samples were performed using limma[28] as previously described[29].

Results

STMN2 protein is extremely sensitive to stress-induced depletion in human cells

We previously found, using recovery from a reversible stressor sodium arsenite ($NaAsO_2$) as a stress paradigm, that STMN2 depletion correlates with nuclear condensation of TDP-43, loss of its solubility and activation of cryptic splicing[15]. Here, we first confirmed stress-induced STMN2 depletion in human motor neurons – previously demonstrated by qRT-PCR and western blot[15] – using BaseScope® RNA *in situ* hybridisation (ISH) with STMN2 full-length mRNA probes and immunocytochemistry (Fig. 1A,B; Supplementary Fig. 1A). We next investigated whether other stresses associated with nuclear TDP-43 condensation[15] lead to STMN2 protein depletion. The ER stressor thapsigargin and viral infection mimic polyinosinic:polycytidylic acid (p(I:C)) led to nearly complete STMN2 protein loss 3 hours post-treatment or 8 hours post-transfection, respectively (Fig. 1C). A delayed response to p(I:C) was likely due to its delivery by lipofection, requiring more time to build a stress response. In contrast, treatment with a proteasome inhibitor MG132 led to STMN2 protein accumulation (Fig. 1C), consistent with its proteasome-mediated turnover[30]. To test the efficiency of STMN2 clearance under stress, we employed treatment with statins that upregulate stathmins via inhibition of the mevalonate pathway[31] (Supplementary Fig. 1B). SH-SY5Y cells were treated with various concentrations of statins simvastatin or

pitavastatin for 16 hours prior to arsenite stress. Despite substantial STMN2 upregulation in statin-pretreated cells, the protein was still almost completely cleared after 6 hours of recovery (Fig. 1D; Supplementary Fig. 1C,D).

We next performed a detailed analysis of STMN2 mRNA and protein level temporal dynamics and TDP-43 solubility between 1 and 30 hours of recovery from $NaAsO_2$ stress, in SH-SY5Y cells. STMN2 is a very short-lived protein, with a half-life of ~2 hours[30, 32]. It was almost completely depleted after 6 hours of recovery, with complete restoration between 12 and 16 hours of recovery (Fig. 1E,F). STMN2 protein level correlated well with STMN2 mRNA level (Fig. 1G) and with TDP-43 solubility (Fig. 1E), where STMN2 mRNA was reduced to <20% of the basal (non-stressed) level between 6 and 10 hours of recovery (Fig. 1G). Ribopuromycilation assay revealed a global shutdown of protein synthesis between 1 and 3 hours of recovery, with its gradual restoration from 6 h of recovery onward (Fig. 1E,F). Consistently, phospho-eIF2α was dramatically upregulated in this time window (Fig. 1E,F). Despite partial restoration of global translation from 6 hours of recovery, STMN2 protein levels continued to decline (Fig. 1E,F) – which coincided with STMN2 mRNA depletion (Fig. 1G). In contrast, the level of STMN3, that has a very similar half-life[32] but is not regulated by cryptic splicing, was significantly restored at the 6-hour time-point (Supplementary Fig.1E,F). Therefore, STMN2 protein loss in stressed cells is driven by both the suppression of protein synthesis and low STMN2 mRNA availability.

We also analysed the dynamics of other ALS-relevant proteins under the same stress conditions. The levels of the relatively stable RNA-binding proteins HuR/ELAVL1 and MATR3 (half-live of >40 hours) did not change during the recovery from arsenite stress. A relatively short-lived protein OPTN (half-life of ~8 hours)[33] remained stable under these conditions (Supplementary Fig. 1E,F).

We next studied the *Stmn2* gene regulation under stress in the mouse cells (Neuro2a) that lack the TDP-43-regulated cryptic exon (CE) element[1] (Supplementary Fig.2A). First, we confirmed that mouse Tdp-43 also forms nuclear condensates during the recovery from $NaAsO_2$ stress, with a similar temporal dynamics as in human cells (Supplementary Fig. 2B). Both Stmn2 mRNA and protein levels were sustained during stress and recovery in mouse cells (Supplementary Fig. 2C,D). Surprisingly, we found that mouse cells have a much shorter period of translation inhibition than human cells – with protein synthesis abolished only at the 1-hour recovery time-point and significantly restored from 3 h of recovery (Supplementary Fig. 2E). Therefore, mouse cells differ

from human cells in their regulation of STMN2 under stress, not only due to lack of cryptic splicing in this gene but also due to shorter translation suppression.

Early in stress, STMN2 is rapidly cleared by the proteasome and is phosphorylated

To establish the primary route of STMN2 protein clearance during stress, SH-SY5Y cells were treated with MG132 or autophagosome-lysosome inhibitor chloroquine (CQ), prior to $NaAsO_2$ addition. MG132 but not CQ prevented STMN2 depletion between 1 and 6 hours of recovery (Fig. 2A). Using a proteasome activity probe, Me4BodipyFL-Ahx3leu3VS that detects proteolytically active proteasome subunits[34], we found that proteasome activity increases very early during stress (30 min of $NaAsO_2$), before declining during the recovery period (at 45 min) (Fig. 2B). Consistently, we observed significant STMN2 protein depletion as early as 20 min into stress exposure (Fig. 2C,D). This coincided with a loss of STMN2 clustered localisation, where it became diffusely distributed in the cytosol (Fig. 2D). Upon translation block with cycloheximide, to uncouple protein synthesis and degradation, STMN2 level at 1 hour of recovery was higher in stressed compared to non-stressed cells (Supplementary Fig. 3A), supporting that proteasome activity declines at this time-point. MG132 pre-treatment also prevented STMN2 depletion at these early time-points (Supplementary Fig. 3B).

In addition to its depletion, STMN2 protein underwent a shift to a slower migrating band from 50-60 min of $NaAsO_2$ stress, suggestive of a post-translational modification (PTM) (Fig. 2A,C). This shift was also detectable with other stressors (Fig. 1C). Stathmins are phosphoproteins whose phosphorylation leads to reduced binding to tubulin and loss of function in tubulin sequestration[35]. Phosphorylation was associated with a functionally inactive STMN2 state[36]. Treatment of SH-SY5Y cell lysates from control and stressed cells with calf intestinal alkaline phosphatase (CIP) reversed the STMN2 mobility change to the control level (Fig. 2E), confirming that STMN2 undergoes extensive phosphorylation under stress. We next asked whether this PTM influences stress-induced STMN2 clearance. We generated constructs to express C-terminally GFP-tagged STMN2 and its non-phosphorylatable form (3A) – with three serines in the proline-rich domain (PrD) mutated to alanines, including the two most frequently phosphorylated ones (Ser-62, Ser-73)[37] (Fig. 2F). Tagged STMN2 displayed a typical clustered localisation, and STMN2-3A variant was expressed and distributed similar to the WT protein (Fig. 2G). Loss of phosphorylation on these sites did not affect the rate of STMN2 clearance during stress (Fig. 2H).

STMN2 prominently localises to the Golgi apparatus membranes[38]. Using a Golgi marker GM130, we confirmed that STMN2 loses its localisation to Golgi early during stress (30

min), including in human motor neurons, which was accompanied by Golgi fragmentation (Fig. 2I,J).

Thus, STMN2 is subject to extremely rapid and drastic changes in its abundance, localisation and functional state early during stress (on the scale of minutes), which precedes its regulation via TDP-43-controlled cryptic splicing.

STMN2 protein synthesis remains active under acute stress

In the course of above studies, we made an unexpected observation that despite the dramatic depletion of STMN2 protein between 30 and 60 min of arsenite exposure, it is restored to ~75% of the pre-stress level after 1 hour of recovery, before being depleted again; this was observed both in neuroblastoma cells and human motor neurons (Fig. 3A,B; Supplementary Fig. 3C). This effect was not due to fluctuations in STMN2 solubility, since this depletion was detectable after urea extraction/solubilisation (Supplementary Fig. 3D). This phenotype was confirmed using an independent STMN2 antibody (Supplementary Fig. 3E). This finding and the fact that STMN2 mRNA is relatively stable (Fig. 1G) suggested that STMN2 protein is actively synthesised during stress despite global translation shutdown. To selectively measure STMN2 translation, we employed proximity ligation assay coupled with puromycin labelling (puro-PLA), which allows quantitative detection of the individual protein molecule synthesis *in situ*[39] (Fig. 3C). STMN2 protein synthesis could be readily detected under basal conditions (>100 PLA signals per cell; 10-min puromycin pulse) but was completely abolished by cycloheximide co-treatment and was severely reduced after 1 hour of stress (Fig. 3D; Supplementary Fig. 3F). However, accumulation of the puro-PLA signal for 30 min during the recovery (continuous puromycin presence in the media between 10 and 40 min of recovery), allowed the detection of ongoing STMN2 translation – which remained at ~30% of the basal level (Fig. 3D). *STMN2* gene sequence analysis for putative IRES and other elements failed to identify any regulatory elements that may underlie active STMN2 translation during stress (data not shown). Interestingly, STMN2 mRNA lacks a Kozak consensus sequence. Notably, when the proteasome was inhibited in stressed cells, STMN2 protein accumulated at a level higher than in non-stressed cells (Supplementary Fig. 3B; compare 1- or 3-hour recovery time-points with and without MG132), supporting its ongoing synthesis under the conditions of declining proteasome activity.

STMN2 translation is modulated by stress granules

We noticed that STMN2 undergoes rapid depletion in chloroquine (CQ)-treated cells in the absence of $NaAsO_2$ stress – being dramatically downregulated after just 1 hour of pre-

treatment (Fig. 2A). Similar to other chemical treatments examined here ($NaAsO_2$, thapsigargin, p(I:C)), CQ can induce eIF2α phosphorylation typical for activation of integrated stress response[40]. This led us to hypothesise that treatments associated with translational repression serve as a signal for rapid STMN2 depletion. We asked whether stressors that repress translation via an alternative mechanism, not involving eIF2α phosphorylation, would also affect STMN2 protein (Fig. 4A). Small molecule inhibitors of another translation initiation factor, eIF4A, silvestrol and rocaglamide-A[41] both caused dramatic depletion of STMN2 within only 1 hour of treatment, being more efficient than phosho-eIF2α-dependent stressors sorbitol and thapsgargin tested in parallel (Fig. 4B,C).

A common denominator for all of the above treatments is the assembly of stress granules (SGs)[42] – RNP condensates thought to be involved in translational repression and dysregulated in neurodegeneration[43] (Fig. 4A,D). We hypothesised that SGs contribute to the regulation of STMN2 protein levels under stress. First, we employed single-molecule (sm)RNA-FISH to study STMN2 mRNA enrichment in SGs. In line with high STMN2 abundance in neuronal cells, high-density mRNA signal was detected, with individual mRNA molecules barely distinguishable; visible segregation of these single-molecule signals into clusters/foci was observed in $NaAsO_2$-treated cells (Fig. 4E). For quantification of STMN2 mRNA enrichment in SGs, they were visualised using ectopic expression of G3BP1-GFP. Quantification of STMN2 mRNA signal intensity within SGs and in SG-free cytosol demonstrated that STMN2 mRNA is, on average, 1.32-fold enriched in SGs compared to the surrounding cytosol (Fig. 4F). Although SG are generally believed to repress translation of sequestered mRNAs[44], some studies indicate that translation in SGs is not uncommon[45]. We used puro-PLA in G3BP1-GFP expressing cells at the 1-hour recovery time-point (when STMN2 protein level is high) to track the origin of the newly synthesised STMN2 protein molecules. STMN2 puro-PLA signals were found almost exclusively outside SGs (Fig. 4G), indicating that STMN2 mRNA translation is inhibited within SGs, consistent with the canonical role for SGs in translation repression. Notably however, a substantial number of STMN2 mRNA molecules were found outside microscopically visible SGs (measured as higher RNA-FISH signal intensity in the cytosol compared to the background outside cells) (Fig. 4F). Presumably, this non-SG pool is responsible for STMN2 protein synthesis under stress (Fig. 3D).

To directly address the role of SGs in limiting STMN2 protein synthesis in stressed cells, we utilised two small molecule inhibitors of SG assembly – ISRIB[46] and lipoamide[47]. ISRIB acts downstream of phospho-eIF2α mediated stress signalling, by increasing active eIF2B subunit assembly and reversing the effects of the eIF2α phosphorylation event, inhibiting SG assembly as a result[48]. In contrast, lipoamide directly attenuates SG condensation by changing the redox state of RNA-binding proteins – SG components. Longitudinal analysis

with automated quantification demonstrated that pre-treatment with either compound reduces $NaAsO_2$-induced SG assembly in SH-SY5Y cells, with ISRIB being more potent than lipoamide (Fig. 4H; Supplementary Fig. 4A-C). Western blot and immunostaining revealed that both ISRIB and lipoamide promote STMN2 protein accumulation during the recovery from $NaAsO_2$ stress (Fig. 4I; Supplementary Fig. 4D,E).

STMN2 expression is sensitive to mild chronic translation deficits

Chronic impairment of translation efficiency is typical for neurodegenerative diseases[49, 50]. To model persistent yet mild translation deficits, we employed ultra-low concentrations of arsenite. Alongside this, we included a repetitive stress paradigm, where acute stress pulses were followed by periods of recovery (Fig. 5A). For repetitive stress, reduced arsenite concentration and duration of treatment, as compared to the standard acute stress, were used, to ensure adequate cell survival for 48 hours (Fig. 5A). STMN2 protein depletion under these milder conditions was confirmed (Supplementary Fig. 5A). Although STMN2 protein level was fully restored between stress pulses in the repetitive stress paradigm, the protein was significantly depleted in the chronic stress paradigm both in SH-SY5Y cells and human motor neurons – detectable already at 24 hours (Fig. 5B,C; Supplementary Fig. 5B,C). In contrast, HuR/ELAVL1, MATR3 and OPTN were not affected by chronic or repetitive stress (Supplementary Fig. 5D). Chronic exposure of neurons to arsenite at 25-40 µM was previously shown to induce TDP-43 loss-of-function in splicing[51]. Our chronic stress paradigm based on a 10-fold lower arsenite concentration did not lead to visible nuclear TDP-43 condensation, loss of solubility or cytoplasmic redistribution (Fig. 5D). Nor did it cause SG assembly or significantly affect STMN2 mRNA levels (Supplementary Fig. 5E and not shown). Ribopuromycilation revealed attenuated translation and elevated phospho-eIF2α levels during chronic stress (Fig. 5E; Supplementary Fig. 5B). Although more stable in neurons as compared to SH-SY5Y cells (~2 hours vs. ~50 min) (Fig. 5F), STMN2 is among the most short-lived proteins in human cells[52].

Phenotypically, chronic, but not repetitive, stress caused Golgi complex disruption in neurons, with STMN2 dissociation and redistribution (Fig. 5G). Longitudinal analysis on Incucyte showed that chronic but not repetitive stress leads to a dramatic increase in apoptosis in both SH-SY5Y cells and human motor neurons (Fig. 5H,I; Supplementary Fig. 5F).

Thus, chronic stress states with impaired protein translation are associated with STMN2 protein downregulation in the absence of detectable TDP-43 pathology.

Pre-stress STMN2 protein levels modulate cell survival under stress

We next asked whether altered levels of STMN2 protein would affect neuronal fitness and survival under stress. First, we performed survival analysis in SH-SY5Y cells transfected with STMN2-specific or scrambled siRNA. Successful STMN2 knockdown was confirmed by western blot in cultures prepared in parallel (Fig. 6A). Cells were subjected to $NaAsO_2$ stress at 24 h post-transfection for 1 hour, and cell proliferation rates and apoptosis rates were monitored by automated imaging on Incucyte for 24 hours of recovery. STMN2 depletion *per se* was well-tolerated by neuroblastoma cells and did not significantly affect their proliferation or viability (Fig. 6B). However, STMN2 siRNA-transfected cells demonstrated a significant increase in cell death (apoptotic cell count) and decrease in proliferation rate (confluency) post-stress, as compared to the scrambled control (Fig. 6B).

In order to perform a reciprocal experiment, we utilised lentiviral expression of untagged STMN2. As a control, we used expression of an unrelated protein, Cry2olig[23]. Low and high virus titres (MOI of 2 and 10, respectively) for STMN2 and control were included in these experiments. Firstly, we confirmed successful STMN2 overexpression using immunocytochemistry and western blot (48 hours post-transduction; Fig. 6C). Moderate STMN2 overexpression achieved with MOI2 (~3-fold upregulation over the endogenous) was well-tolerated by neuroblastoma cells, whereas the high titre (MOI10) led to significant toxicity (Supplementary Fig. 6). It should be noted that although the levels of STMN2 and control protein could not be directly compared, the toxicity in the MOI2 STMN2 cultures was similar to that in the MOI10 control cultures (Supplementary Fig. 6). For survival analysis under stress, we used the non-toxic MOI2. Transduced cultures were subjected to acute arsenite stress (1 hour) at 48 h post-transduction and monitored for 24 hours of recovery. STMN2 transduced cultures were found to be partially protected from stress-induced apoptosis compared to the Cry2olig control (Fig. 6D).

Since statins efficiently upregulate STMN2[31], we studied the effect of statin pre-treatment on cellular survival under stress. Of note, we found that statins at concentrations >500 nM promote neuron-like phenotypes in neuroblastoma cells – most notably, neurite outgrowth (Supplementary Fig. 1C), which could confound confluency measurements. Therefore, lower statin concentrations not associated with visible morphological changes were employed. Cells were pre-treated with 100, 250 or 500 nM pitavastatin for 16 hours and subjected to arsenite stress. Apoptosis analysis revealed a protective effect of pitavastatin pre-treatment during the recovery from $NaAsO_2$ stress, in a concentration-dependent manner (Fig. 6E).

Therefore, genetic or pharmacological manipulation of the pre-stress STMN2 protein level is sufficient to modulate cell survival under stress, where STMN2 upregulation is protective.

STMN2 expression compensation at the RNA level in ALS

STMN2 studies in human post-mortem samples were primarily focused on STMN2 CE-containing RNA; we were able to find only two studies that measured STMN2 protein, one by immunochemistry and one – by single-cell proteomics[1, 53]. We tested two commercial anti-STMN2 antibodies, rabbit polyclonal and mouse monoclonal (Proteintech), which both performed well in immunocytochemistry and recognised a single band in western blot. The rabbit antibody provided a stronger staining of spinal motor neurons than the mouse antibody, albeit with some background including astrocyte and neuropil labelling, but no lipofuscin detection (Fig. 7A, Supplementary Fig. 7A). Given a prominent signal in motor neurons, this antibody was used for a systematic analysis of STMN2 protein levels in ALS spinal motor neurons. Firstly, a cohort of sporadic ALS (sALS) cases with confirmed TDP-43 pathology ([54] and Supplementary Fig. 7B) was analysed (n=5 per group). Automated analysis of STMN2 pixel intensity using QuPath demonstrated significant STMN2 downregulation in the surviving motor neurons in sALS as compared to controls (Fig. 7A,B). We were also able to visualise STMN2 mRNA depletion in sALS motor neurons using BaseScope ISH (Fig. 7C).

Since our cellular findings suggested that STMN2 can be misregulated via mechanisms other than TDP-43 loss-of-function, we performed STMN2 protein analysis in a cohort of non-TDP ALS cases, ALS-FUS and ALS-SOD1. Both ALS subtypes are characterised by altered translation and/or SG-related pathology[55-61]. Two ALS-SOD1 and three ALS-FUS cases were included in the study[62, 63]. One of the ALS-FUS cases was a new, unpublished case (p.Pro525Arg) with abundant FUS pathology. Therefore, our panel of ALS-FUS cases broadly represented the ALS-FUS subtype, with both late- and early-onset cases included. Although spinal neurons in non-TDP ALS cases tended to have variable STMN2 protein expression, on average, they showed no significant depletion, as compared to controls (Fig. 7D).

To address the mechanisms of STMN2 protein expression maintenance in non-TDP ALS, we utilised cellular models. Consistent with the ALS-FUS tissue data, STMN2 protein level was maintained in our FUSΔNLS cells, both under basal conditions and under stress (Fig. 8A; Supplementary Fig. 8A), despite a stress-mimicking state in these lines (i.e. phospho-eIF2α upregulation) (Supplementary Fig. 8B). This led us to hypothesise that in non-TDP ALS, the defects in STMN2 protein production due to misregulation of protein translation/SG may be compensated at the RNA level. To interrogate this, we re-analysed published RNA-seq data from ALS-FUS cell models. Indeed, STMN2 mRNA levels were found upregulated in two neuroblastoma cell models – FUSΔNLS lines (both homo- and heterozygous)[27] and in a cell

line with inducible expression of the P525L variant[64] (Fig. 8B). Furthermore, STMN2 mRNA was also upregulated in iPSC-derived motor neurons with heterozygous expression of the P525L mutant (single-cell RNA-seq)[65] (Fig. 8B). In contrast, STMN1 and STMN3 did not show differential expression in ALS-FUS models. Finally, we also detected STMN2 pre-mRNA upregulation in FUSΔNLS cells (Fig. 8C).

TDP-43 dysfunction itself can result in translation and SG deficits[66-69], therefore such mRNA-level compensation may also occur in this subtype at the early disease stages, before the onset of TDP-43 proteinopathy. We performed STMN2 mRNA analysis in human post-mortem tissue from sALS patients and healthy controls using bulk RNA-seq datasets from the New York Genome Center (NYGC) ALS Consortium (~200 cases). Motor cortex, frontal cortex and spinal cord were included in this analysis. STMN2 mRNA was found significantly upregulated in the ALS frontal cortex (*padj=0.0025), with a trend towards STMN2 upregulation in the motor cortex (padj=0.08227) – the two areas that are relatively spared in the disease, with no difference in the spinal cord (Fig. 8D). Consistently, we also detected a trend towards STMN2 mRNA upregulation in the motor cortex in a small (n=4) cohort of ALS-C9 cases using qRT-PCR (Fig. 8E). Interestingly, ALS-C9 cases in this latter sample set displayed dramatic STMN2 CE accumulation (Fig. 8E). Finally, STMN2 mRNA was marginally upregulated in the frontal cortex of ALS-SOD1 patients (6 cases) in the NYGC ALS cohort (non-adjusted p-value=0.0266) (Supplementary Fig. 9). This dataset contained only one ALS-FUS case precluding meaningful analysis for this ALS subtype.

Discussion

Our detailed analysis of STMN2 regulation under acute and chronic stress reveals how intrinsic sensitivity of STMN2 protein synthesis to stress-induced molecular changes can create a vulnerable neuronal state (Fig. 8F). Our findings implicate two common denominators of ALS – misregulation of protein translation and SGs – in STMN2 downregulation, independently of TDP-43 loss of function in splicing (Fig. 8F).

Here, we describe the “early” (minutes) and “late” (hours) mechanisms of STMN2 depletion during stress. STMN2 depletion/inactivation can occur within minutes after the exposure to stressor and independently of cryptic splicing – via activated proteasomal degradation, SG-mediated translation repression and, potentially, phosphorylation. Enhanced STMN2 degradation may represent a side-effect of stress-induced proteasome activation – required to prevent the build-up of misfolded proteins during stress[70]. Likewise, STMN2 translation suppression by SGs may be secondary to their role in selective translation

critical for proteostasis maintenance under stress[43]. Thus, these two broadly cytoprotective mechanisms may lead to "unintentional", non-specific STMN2 reduction during stress. In contrast, STMN2 phosphorylation was identified as a targeted, physiological mechanism of its functional inactivation, through prevention of tubulin binding[36, 71]. However, a recent study suggested that tubulin binding by STMN2 is dispensable for axonal regeneration[72]. Therefore, phosphorylation under stress may not be linked to *regulated* loss of STMN2 activity, instead representing a side-effect of increased kinase activity. On the other hand, we show that STMN2 protein synthesis can withstand stress-induced translation shutdown, remaining high during stress (~30% of basal), which is likely facilitated by the exceptional abundance of its mRNA[1]. Therefore, post-transcriptional (TDP-43-dependent cryptic splicing and SGs) and post-translational (phosphorylation) regulation of STMN2 levels/activity may represent physiological mechanisms – presumably more controllable and fail-safe than regulation of the translational output of the *STMN2* gene. However, if these mechanisms are dysregulated in disease, STMN2 expression would suffer significantly. We also show that human and mouse cells significantly differ in STMN2 regulation under stress, both through TDP-43-dependent and -independent mechanisms, which should be taken into account in future studies.

We find that STMN2 expression is significantly impacted by chronic translation deficits. Consistently, in a recent study using machine learning analysis of proteomic datasets, a decrease in ribosomal protein RPS29, and associated STMN2 protein downregulation, was identified as a shared feature of ALS cell models[73]. STMN2's sensitivity to prolonged reduction in protein synthesis is likely due to its extremely rapid turnover. Short-lived proteins, defined as those with a half-live ≤8 hours, account for only ~5% of the human proteome, most of which are low-abundance, regulatory proteins involved in signalling and cell cycle regulation[52]. Short half-life enables efficient control but also increases vulnerability to pathological states with impaired translation.

Misregulation of SGs has been reported across several neurodegenerative diseases[74]. Although SG assembly is typical for acute stress response[75], chronic stress states may lead to submicroscopic RNP granulation/condensation – coalescence of pre-existing RNP complexes under stress[76, 77]. SG regulation is very different in cultured cells and *in vivo* as well as in neuronal vs. non-neuronal cells. Indeed, SG induction has only been achieved in a handful of live animal models, requiring the use of harsh, terminal stresses[24, 78, 79]. Similarly, neurons appear to be more resistant to the assembly of (large) SGs[24, 80]. Submicroscopic RNP condensation may play an important role in STMN2 regulation via translational repression *in vivo*, including in disease (Fig. 8F). Some recent studies questioned the SG role in global translation repression[45, 81]. Our data indicate that SG

function in translation is transcript- and cell type-specific, where the highly abundant, actively translated neurospecific STMN2 mRNA is sensitive to SG formation. Interestingly, in our studies, we noticed that endogenous STMN2 protein was consistently enriched in cytoplasmic foci, which were confirmed to correspond to SGs using anti-G3BP1 co-staining (Supplementary Fig. 10). However, we were unable to confirm STMN2 enrichment in SGs using ectopically expressed GFP- or V5-tagged STMN2 (Supplementary Fig. 10). Thus, some anti-STMN2 antibodies non-specifically recognise SGs in immunostaining, which should be taken into account in future studies.

Importantly, we find that pre-stress STMN2 protein level significantly modulates cellular viability under stress – where its higher level is protective and reduced level sensitises against stress-induced apoptosis. This suggests that cells with depleted STMN2 exist in a fragile state – where their vulnerability is exposed by stress. Therefore, STMN2 depletion by (chronic) stress amplifies the toxicity of subsequent stresses.

Restoration of protein synthesis using small molecules has long been considered an attractive therapeutic strategy in neurodegenerative diseases, including ALS[82]. Some of such translation activators lead to SG dissolution[83]. For example, DNL343, an investigational small-molecule drug with a mechanism of action similar to that of ISRIB, showed promise in reversing pathological phenotypes in TDP-43 transgenic mice[84]. Other compounds, with less favourable pharmacokinetic profiles, also showed promise in earlier reports[85, 86]. Their beneficial effect may be at least partially mediated by STMN2 maintenance/restoration.

Our cellular and human tissue data suggest that STMN2 is subject to expression compensation at the RNA level in ALS – which may be sufficient to counteract protein translation impairment in non-TDP ALS such as ALS-FUS. We find evidence for such compensation in the CNS regions in ALS-TDP that are relatively spared pathologically (cortex), but not in those with profound TDP-43 pathology (spinal cord). In the severely affected spinal cord, this compensation likely fails due to cryptic splicing. Since TDP-43 itself is involved in SG metabolism and translation regulation[69, 87-89], its pathology would create a vicious cycle of cellular dysfunction. Interestingly, STMN2 mRNA upregulation was reported in ALS-SOD1 mice[90]. STMN2 preservation in ALS-FUS and -SOD1 may ameliorate the disease course in these ALS subtypes. Yet, pathological changes in these subtypes still develop and progress, despite STMN2 preservation. This suggests that multi-target interventions may be required to achieve a *significant* therapeutic effect in ALS.

In conclusion, we demonstrate that molecular pathologies other than TDP-43 dysfunction converge on STMN2 and provide an additional mechanism for neuronal impairment by abnormal translation and SG regulation.

Data availability

The authors confirm that the data supporting the findings of this study are available within the article and its supplementary material.

Acknowledgements

We are grateful to the Sheffield Brain Tissue Bank for supplying human tissue and to the NYGC ALS consortium for providing datasets for analysis. We thank those who have donated tissue for scientific research and their families who have supported this. We also thank Dan Fillingham for assisting with human tissue preparation, David Burrows for the help with Neuro2A cell culture and Emily Day for the help with image processing. We are grateful to Ze'ev Melamed, Guillaume Hautbergue and Alison Twelvetrees for useful discussions. The thumbnail image for the online table of contents was created in BioRender. Shelkovnikova, T. (2026) https://BioRender.com/zawd4u5.

Funding

The work was supported by the UKRI Future Leaders Fellowship (MR/W004615/1), responsive mode grants from the MRC (MR/W028522/1) and BBSRC (BB/V014110/1), MND Association fellowship/grant (968-799), and Alzheimer's Research UK pilot grant (ARUK-PPG2023B-007) to T.A.S. B.S.C.E. was supported by a PhD studentship from the MND Scotland (2022/MNDS/PHD/8045SHEL; to T.A.S. and K.J.D.V.). E.D. and V.K. are funded by PhD studentships from the University of Sheffield Faculty of Health and Neuroscience Institute, respectively (to T.A.S.). M.N. was supported by the Association for Frontotemporal Degeneration Holloway Postdoctoral Fellowship, The Cullen Education and Research Foundation, and Hop On a Cure. J.R.H. acknowledges funding from The Pathological Society of Great Britain and Ireland and the MND Association. R.J.H.W. and J.C.K. are supported by Tambourine's ALS Breakthrough Research Fund in partnership with the Milken Institute Center for Strategic Philanthropy. J.C.K. is also supported through the Lister Institute Research Prize.

Competing interests

C.L.T. and M.N. have filed patent applications related to the use of statins in neurodegenerative diseases. Other authors declare no competing interests.

Supplementary material

Supplementary material is available at *Brain* online.

References

1. Klim, J.R. *et al.* ALS-implicated protein TDP-43 sustains levels of STMN2, a mediator of motor neuron growth and repair. *Nat Neurosci* 2019;22:167-179 doi; 10.1038/s41593-018-0300-4

2. Melamed, Z. *et al.* Premature polyadenylation-mediated loss of stathmin-2 is a hallmark of TDP-43-dependent neurodegeneration. *Nat Neurosci* 2019;22:180-190 doi; 10.1038/s41593-018-0293-z

3. Agra Almeida Quadros, A.R. *et al.* Cryptic splicing of stathmin-2 and UNC13A mRNAs is a pathological hallmark of TDP-43-associated Alzheimer's disease. *Acta Neuropathol* 2024;147(9) doi;10.1007/s00401-023-02655-0

4. Baughn, M.W. *et al.* Mechanism of STMN2 cryptic splice-polyadenylation and its correction for TDP-43 proteinopathies. *Science* 2023;379:1140-1149 doi;10.1126/science.abq5622

5. Wen, H.L. *et al.* Stathmin, a microtubule-destabilizing protein, is dysregulated in spinal muscular atrophy. *Human molecular genetics* 2010;19:1766-1778 doi;10.1093/hmg/ddq058

6. Wang, Q. *et al.* The landscape of multiscale transcriptomic networks and key regulators in Parkinson's disease. *Nat Commun* 2019;10:5234 doi;10.1038/s41467-019-13144-y

7. San Juan, I.G. *et al.* Loss of mouse Stmn2 function causes motor neuropathy. *Neuron* 2022;110:4031 doi;10.1016/j.neuron.2022.02.011

8. Liedtke, W., Leman, E.E., Fyffe, R.E., Raine, C.S. & Schubart, U.K. Stathmin-deficient mice develop an age-dependent axonopathy of the central and peripheral nervous systems. *Am J Pathol* 2002;160:469-480 doi;10.1016/S0002-9440(10)64866-3

9. Krus, K.L. *et al.* Loss of Stathmin-2, a hallmark of TDP-43-associated ALS, causes motor neuropathy. *Cell Rep* 2022;39:111001 doi;10.1016/j.celrep.2022.111001

10. Zhu, X.X. *et al.* Molecular cloning of a novel human leukemia-associated gene. Evidence of conservation in animal species. *The Journal of biological chemistry* 1989;264:14556-14560

11. Sun, S. *et al.* Translational profiling identifies a cascade of damage initiated in motor neurons and spreading to glia in mutant SOD1-mediated ALS. *Proc Natl Acad Sci U S A* 2015;112:E6993-7002 doi;10.1073/pnas.1520639112

12. Sobel, A. *et al.* Intracellular substrates for extracellular signaling. Characterization of a ubiquitous, neuron-enriched phosphoprotein (stathmin). *The Journal of biological chemistry* 1989;264(7):3765-3772

13. Shin, J.E., Geisler, S. & DiAntonio, A. Dynamic regulation of SCG10 in regenerating axons after injury. *Exp Neurol* 2014;252:1-11 doi;10.1016/j.expneurol.2013.11.007

14. Morii, H., Shiraishi-Yamaguchi, Y. & Mori, N. SCG10, a microtubule destabilizing factor, stimulates the neurite outgrowth by modulating microtubule dynamics in rat hippocampal primary cultured neurons. *J Neurobiol* 2006;66:1101-1114 doi;10.1002/neu.20295

15. Huang, W.P. *et al.* Stress-induced TDP-43 nuclear condensation causes splicing loss of function and STMN2 depletion. *Cell Rep* 2024;43:114421 doi;10.1016/j.celrep.2024.114421

16. Al-Chalabi, A. *et al.* Analysis of amyotrophic lateral sclerosis as a multistep process: a population-based modelling study. *The Lancet. Neurology* 2014;13:1108-1113 doi;10.1016/S1474-4422(14)70219-4

17. Gerovska, D. *et al.* Genealogy of the neurodegenerative diseases based on a meta-analysis of age-stratified incidence data. *Sci Rep* 2020;10:18923 doi;10.1038/s41598-020-75014-8

18. Chapman, L., Cooper-Knock, J. & Shaw, P.J. Physical activity as an exogenous risk factor for amyotrophic lateral sclerosis: a review of the evidence. *Brain : a journal of neurology* 2023;146:1745-1757 doi;10.1093/brain/awac470

19. Shelkovnikova, T.A. *et al.* Antiviral Immune Response as a Trigger of FUS Proteinopathy in Amyotrophic Lateral Sclerosis. *Cell Rep* 2019;29:4496-4508 doi;10.1016/j.celrep.2019.11.094

20. Bellmann, J. *et al.* Viral Infections Exacerbate FUS-ALS Phenotypes in iPSC-Derived Spinal Neurons in a Virus Species-Specific Manner. *Front Cell Neurosci* 2019;13:480 doi;10.3389/fncel.2019.00480

21. Yang, J. *et al.* The SARS-CoV-2 main protease induces neurotoxic TDP-43 cleavage and aggregates. *Signal Transduct Target Ther* 2023;8:109. doi;10.1038/s41392-023-01386-8 doi;10.1038/s41392-023-01386-8

22. Hipp, M.S., Kasturi, P. & Hartl, F.U. The proteostasis network and its decline in ageing. *Nat Rev Mol Cell Biol* 2019;20:421-435 doi;10.1038/s41580-019-0101-y

23. Hodgson, R.E. *et al.* C9orf72 poly-PR forms anisotropic condensates causative of nuclear TDP-43 pathology. *iScience* 2024;27:110937 doi;10.1016/j.isci.2024.110937

24. Shelkovnikova, T.A. *et al.* Chronically stressed or stress-preconditioned neurons fail to maintain stress granule assembly. *Cell Death Dis* 2017;8:e2788 doi;10.1038/cddis.2017.199

25. Shelkovnikova, T.A. *et al.* Protective paraspeckle hyper-assembly downstream of TDP-43 loss of function in amyotrophic lateral sclerosis. *Mol Neurodegener* 2018;13:30 doi; 10.1186/s13024-018-0263-7

26. An, H. *et al.* A toolkit for the identification of NEAT1_2/paraspeckle modulators. *Nucleic Acids Res* 2022;50:e119 doi;10.1093/nar/gkac771

27. An, H. *et al.* ALS-linked FUS mutations confer loss and gain of function in the nucleus by promoting excessive formation of dysfunctional paraspeckles. *Acta Neuropathol Commun* 2019;7:7 doi;10.1186/s40478-019-0658-x

28. Ritchie, M.E. *et al.* limma powers differential expression analyses for RNA-sequencing and microarray studies. *Nucleic Acids Res* 2015;43:e47 doi;10.1093/nar/gkv007

29. Humphrey, J. *et al.* Integrative transcriptomic analysis of the amyotrophic lateral sclerosis spinal cord implicates glial activation and suggests new risk genes. *Nat Neurosci* 2023;26:150-162 doi;10.1038/s41593-022-01205-3

30. Deng, X., Bradshaw, G., Kalocsay, M. & Mitchison, T. Tubulin Regulates the Stability and Localization of STMN2 by Binding Preferentially to Its Soluble Form. *bioRxiv* (2025) doi; 10.1101/2025.02.27.640326

31. Nolan, M. *et al.* Statins and genetic inhibition of the mevalonate pathway activate an ATF3-STMN2 regenerative program. *bioRxiv* (2026) doi;10.64898/2026.02.23.707492

32. Thornburg-Suresh, E.J.C., Richardson, J.E. & Summers, D.W. The Stathmin-2 membrane-targeting domain is required for axon protection and regulated degradation by DLK signaling. *The Journal of biological chemistry* 2023;299: 104861 doi;10.1016/j.jbc.2023.104861

33. Shen, X. *et al.* Processing of optineurin in neuronal cells. *The Journal of biological chemistry* 2011;286: 3618-3629 doi;10.1074/jbc.M110.175810

34. Berkers, C.R. *et al.* Profiling proteasome activity in tissue with fluorescent probes. *Mol Pharm* 2007;4: 739-748 doi;10.1021/mp0700256

35. Dar, S.A. *et al.* Full-length direct RNA sequencing uncovers stress-granule dependent RNA decay upon cellular stress. *eLife* 2024;13:RP96284 doi;10.7554/eLife.96284

36. Steinmetz, M.O. *et al.* Phosphorylation disrupts the central helix in Op18/stathmin and suppresses binding to tubulin. *EMBO Rep* 2001;2: 505-510 doi;10.1093/embo-reports/kve105

37. Tararuk, T. *et al.* JNK1 phosphorylation of SCG10 determines microtubule dynamics and axodendritic length. *J Cell Biol* 2006;173: 265-277 doi;10.1083/jcb.200511055

38. Di Paolo, G. *et al.* Targeting of SCG10 to the area of the Golgi complex is mediated by its NH2-terminal region. *The Journal of biological chemistry* 1997;272:5175-5182 doi;10.1074/jbc.272.8.5175

39. tom Dieck, S. *et al.* Direct visualization of newly synthesized target proteins in situ. *Nat Methods* 2015;12:411-414 doi;10.1038/nmeth.3319

40. Tian, A.L. *et al.* Lysosomotropic agents including azithromycin, chloroquine and hydroxychloroquine activate the integrated stress response. *Cell Death Dis* 2021;12:6 doi;10.1038/s41419-020-03324-w

41. Naineni, S.K. *et al.* Protein-RNA interactions mediated by silvestrol-insight into a unique molecular clamp. *Nucleic Acids Res* 2024;52: 12701-12711 doi;10.1093/nar/gkae824

42. Hofmann, S., Kedersha, N., Anderson, P. & Ivanov, P. Molecular mechanisms of stress granule assembly and disassembly. *Biochim Biophys Acta Mol Cell Res* 2021; **1868**:118876 doi;10.1016/j.bbamcr.2020.118876

43. Buchan, J.R. & Parker, R. Eukaryotic stress granules: the ins and outs of translation. *Molecular cell* 2009;36:932-941 doi;10.1016/j.molcel.2009.11.020

44. Baymiller, M. & Moon, S.L. Stress Granules as Causes and Consequences of Translation Suppression. *Antioxid Redox Signal* 2023; 39:390-409

45. Mateju, D. *et al.* Single-Molecule Imaging Reveals Translation of mRNAs Localized to Stress Granules. *Cell* 2020; 183:1801-1812 e1813 doi;10.1016/j.cell.2020.11.010

46. Sidrauski, C. *et al.* Pharmacological brake-release of mRNA translation enhances cognitive memory. *Elife* 2013;2:e00498 doi;10.7554/eLife.00498

47. Uechi, H. *et al.* Small-molecule dissolution of stress granules by redox modulation benefits ALS models. *Nat Chem Biol* 2025;10:1577-1588 doi;10.1038/s41589-025-01893-5

48. Zyryanova, A.F. *et al.* ISRIB Blunts the Integrated Stress Response by Allosterically Antagonising the Inhibitory Effect of Phosphorylated eIF2 on eIF2B. *Molecular cell* 2021;81:88-103 e106 doi;10.1016/j.molcel.2020.10.031

49. Lehmkuhl, E.M. & Zarnescu, D.C. Lost in Translation: Evidence for Protein Synthesis Deficits in ALS/FTD and Related Neurodegenerative Diseases. *Adv Neurobiol* 2018;20:283-301 doi;10.1007/978-3-319-89689-2_11

50. Luh, L.M. & Bertolotti, A. Potential benefit of manipulating protein quality control systems in neurodegenerative diseases. *Curr Opin Neurobiol* 2020; 61:125-132 doi; 10.1016/j.conb.2020.02.009

51. Casiraghi, V. *et al.* Modeling of TDP-43 proteinopathy by chronic oxidative stress identifies rapamycin as beneficial in ALS patient-derived 2D and 3D iPSC models. *Exp Neurol* 2025;383: 115057 doi;10.1016/j.expneurol.2024.115057

52. Li, J. *et al.* Proteome-wide mapping of short-lived proteins in human cells. *Molecular cell* 2021;81: 4722-4735 e4725 doi;10.1016/j.molcel.2021.09.015

53. Guise, A.J. *et al.* TDP-43-stratified single-cell proteomics of postmortem human spinal motor neurons reveals protein dynamics in amyotrophic lateral sclerosis. *Cell Rep* 2024;43:113636 doi;10.1016/j.celrep.2023.113636

54. Cooper-Knock, J. *et al.* Clinico-pathological features in amyotrophic lateral sclerosis with expansions in C9ORF72. *Brain : a journal of neurology* 2012;135:751-764 doi;10.1093/brain/awr365

55. Gal, J. *et al.* ALS mutant SOD1 interacts with G3BP1 and affects stress granule dynamics. *Acta neuropathologica* 2016;132:563-576 doi;10.1007/s00401-016-1601-x

56. Dormann, D. *et al.* Arginine methylation next to the PY-NLS modulates Transportin binding and nuclear import of FUS. *The EMBO journal* 2012;31:4258-4275 doi;10.1038/emboj.2012.261

57. Mateju, D. *et al.* An aberrant phase transition of stress granules triggered by misfolded protein and prevented by chaperone function. *The EMBO journal* 2017;36: 1669-1687 doi;10.15252/embj.201695957

58. Shelkovnikova, T.A., Robinson, H.K., Southcombe, J.A., Ninkina, N. & Buchman, V.L. Multistep process of FUS aggregation in the cell cytoplasm involves RNA-dependent and RNA-independent mechanisms. *Human molecular genetics* 2014;23:5211-5226 doi;10.1093/hmg/ddu243

59. Birsa, N. *et al.* FUS-ALS mutants alter FMRP phase separation equilibrium and impair protein translation. *Sci Adv* 2021;7:30 doi;10.1126/sciadv.abf8660

60. Kamelgarn, M. *et al.* ALS mutations of FUS suppress protein translation and disrupt the regulation of nonsense-mediated decay. *Proc Natl Acad Sci U S A* 2018;115:E11904-E11913 doi;10.1073/pnas.1810413115

61. Szewczyk, B. *et al.* FUS ALS neurons activate major stress pathways and reduce translation as an early protective mechanism against neurodegeneration. *Cell Rep* 2023;43:112025 doi;10.1016/j.celrep.2023.112025

62. Hewitt, C. *et al.* Novel FUS/TLS mutations and pathology in familial and sporadic amyotrophic lateral sclerosis. *Arch Neurol* 2010;67: 455-461 doi;10.1001/archneurol.2010.52

63. Shaw, P.J. *et al.* CNS tissue Cu/Zn superoxide dismutase (SOD1) mutations in motor neurone disease (MND). *Neuroreport* 1997;8:3923-3927 doi;10.1097/00001756-199712220-00016

64. Mariani, D. *et al.* ALS-associated FUS mutation reshapes the RNA and protein composition of stress granules. *Nucleic Acids Res* 2024;52:13269-13289 doi;10.1093/nar/gkae942

65. Schweingruber, C. *et al.* Single-cell RNA-sequencing reveals early mitochondrial dysfunction unique to motor neurons shared across FUS- and TARDBP-ALS. *Nat Commun* 2025;16:4633 doi;10.1038/s41467-025-59679-1

66. Chu, J.F., Majumder, P., Chatterjee, B., Huang, S.L. & Shen, C.J. TDP-43 Regulates Coupled Dendritic mRNA Transport-Translation Processes in Co-operation with FMRP and Staufen1. *Cell Rep* 2019;29:3118-3133 e3116 doi;10.1016/j.celrep.2019.10.061

67. Piol, D., Robberechts, T. & Da Cruz, S. Lost in local translation: TDP-43 and FUS in axonal/neuromuscular junction maintenance and dysregulation in amyotrophic lateral sclerosis. *Neuron* 2023;111:1355-1380 doi;10.1016/j.neuron.2023.02.028

68. Blokhuis, A.M. *et al*. Comparative interactomics analysis of different ALS-associated proteins identifies converging molecular pathways. *Acta neuropathologica* 2016;132:175-196 doi;10.1007/s00401-016-1575-8

69. Aulas, A. & Vande Velde, C. Alterations in stress granule dynamics driven by TDP-43 and FUS: a link to pathological inclusions in ALS? *Front Cell Neurosci* 2015;9:423

70. Lee, D. & Goldberg, A.L. 26S proteasomes become stably activated upon heat shock when ubiquitination and protein degradation increase. *Proc Natl Acad Sci U S A* 2022;119:e2122482119 doi;10.1073/pnas.2122482119

71. Wittmann, T., Bokoch, G.M. & Waterman-Storer, C.M. Regulation of microtubule destabilizing activity of Op18/stathmin downstream of Rac1. *The Journal of biological chemistry* 2004;279:6196-6203 doi;10.1074/jbc.M307261200

72. Beccari, M.S. *et al*. Stathmin-2 enhances motor axon regeneration after injury independent of its binding to tubulin. *Proc Natl Acad Sci U S A* 2025;122:e2502294122 doi;10.1073/pnas.2502294122

73. Xu, W. *et al*. Machine learning-based proteomics profiling of ALS identifies downregulation of RPS29 that maintains protein homeostasis and STMN2 level. *Commun Biol* **8**, 1177 (2025).

74. Cui, Q., Liu, Z. & Bai, G. Friend or foe: The role of stress granule in neurodegenerative disease. *Neuron* 2024;112:2464-2485 doi;10.1016/j.neuron.2024.04.025

75. Anderson, P. & Kedersha, N. Visibly stressed: the role of eIF2, TIA-1, and stress granules in protein translation. *Cell Stress Chaperones* 2002;7: 213-221

76. Youn, J.Y. *et al*. High-Density Proximity Mapping Reveals the Subcellular Organization of mRNA-Associated Granules and Bodies. *Molecular cell* 2018;69: 517-532 e511 doi;10.1016/j.molcel.2017.12.020

77. Markmiller, S. *et al*. Context-Dependent and Disease-Specific Diversity in Protein Interactions within Stress Granules. *Cell* 2018;172:590-604 e513

78. Dubinski, A. *et al.* Stress granule assembly in vivo is deficient in the CNS of mutant TDP-43 ALS mice. *Human molecular genetics* 2023;32:319-332 doi;10.1093/hmg/ddac206

79. Zhang, X. *et al.* In vivo stress granule misprocessing evidenced in a FUS knock-in ALS mouse model. *Brain : a journal of neurology* 2020;143:1350-1367 doi; 10.1093/brain/awaa076

80. Ratti, A. *et al.* Chronic stress induces formation of stress granules and pathological TDP-43 aggregates in human ALS fibroblasts and iPSC-motoneurons. *Neurobiol Dis* 2020;145: 105051 doi;10.1016/j.nbd.2020.105051

81. Smith, J. & Bartel, D.P. The G3BP stress-granule proteins reinforce the integrated stress response translation programme. *Nat Cell Biol* (2025). 2025;28:135–148 doi;10.1038/s41556-025-01834-3

82. Mercado, G. & Hetz, C. Drug repurposing to target proteostasis and prevent neurodegeneration: accelerating translational efforts. *Brain : a journal of neurology*2017;140:1544-1547 doi;10.1093/brain/awx107

83. Sidrauski, C., McGeachy, A.M., Ingolia, N.T. & Walter, P. The small molecule ISRIB reverses the effects of eIF2alpha phosphorylation on translation and stress granule assembly. *Elife* **4** (2015). 2015;4:e05033 doi;10.7554/eLife.05033

84. Flores, B.N. *et al.* Investigational eIF2B activator DNL343 modulates the integrated stress response in preclinical models of TDP-43 pathology and individuals with ALS in a randomized clinical trial. *Nat Commun* 2025;16:7690 doi;10.1038/s41467-025-63031-y

85. Das, I. *et al.* Preventing proteostasis diseases by selective inhibition of a phosphatase regulatory subunit. *Science* 2015;348:239-242 doi;10.1126/science.aaa4484

86. Halliday, M. *et al.* Partial restoration of protein synthesis rates by the small molecule ISRIB prevents neurodegeneration without pancreatic toxicity. *Cell Death Dis* 2015;6:e1672 doi;10.1038/cddis.2015.49

87. Bjork, R.T., Mortimore, N.P., Loganathan, S. & Zarnescu, D.C. Dysregulation of Translation in TDP-43 Proteinopathies: Deficits in the RNA Supply Chain and Local Protein Production. *Front Neurosci* 2022;16:840357 doi;10.3389/fnins.2022.840357

88. Freibaum, B.D., Chitta, R.K., High, A.A. & Taylor, J.P. Global analysis of TDP-43 interacting proteins reveals strong association with RNA splicing and translation machinery. *Journal of proteome research* 2010;9:1104-1120 doi;10.1021/pr901076y

89. Liu-Yesucevitz, L. *et al*. ALS-linked mutations enlarge TDP-43-enriched neuronal RNA granules in the dendritic arbor. *The Journal of neuroscience : the official journal of the Society for Neuroscience* 2014;34:4167-4174 doi;10.1523/JNEUROSCI.2350-13.2014

90. Bellouze, S. *et al*. Stathmin 1/2-triggered microtubule loss mediates Golgi fragmentation in mutant SOD1 motor neurons. *Mol Neurodegener* 2016;11:43 doi;10.1186/s13024-016-0111-6

Figure legends

Figure 1 STMN2 protein loss under stress is driven by both translational repression and STMN2 mRNA depletion. (**A,B**) STMN2 mRNA depletion in human motor neurons late in stress/recovery visualised with BaseScope ISH (A) and immunostaining (B). Probe #1048241-C1 was used in A. Representative images are shown. Scale bars, 100 µm in A and 10 µm in B. (**C**) Cellular stressors with different mechanism of action cause STMN2 protein depletion. Representative western blots are shown. (**D**) Statin pre-treatment upregulates STMN2 protein but does not prevent its stress-induced clearance. Cells were pre-treated with pitavastatin at the concentration indicated for 16 hours. The recovery time-points from $NaAsO_2$ stress are indicated. (**E,F**) Analysis of STMN2 protein dynamics and translation inhibition during the recovery from $NaAsO_2$ stress. Nascent protein production was analysed by ribopuromycilation. Representative western blot (E) and its quantification (F) are shown. (**G**) STMN2 mRNA depletion and subsequent restoration correlate with STMN2 protein level changes during recovery from stress. N=3, **p<0.01, ***p<0.001, one-way ANOVA with Dunnett's post-hoc test. Graph shows mean±S.E.M. SH-SY5Y cells were used in C-G.

Figure 2 Mechanisms of STMN2 regulation early during stress. (**A**) STMN2 protein depletion during stress is mediated by the proteasome. Cells were pre-treated with the indicated compound for one hour prior to stress and were cultured in the presence of the compound during the recovery. Representative western blot and quantification are shown. N=3, **p<0.01, one-tailed paired *t* test. Graph shows mean±S.D. (**B**) Activation of proteasomal degradation early in stress and its subsequent decline during the recovery

from arsenite stress. Proteasome activity probe was added directly to the media before live imaging on Opera Phenix. Fluorescence intensity was plotted from individual cells. (N=3, n=30; ****p<0.0001, one-way ANOVA with Tukey post-hoc test. (**C,D**) STMN2 protein is redistributed and depleted within minutes of $NaAsO_2$ addition. Representative western blot and its quantification (C) and representative immunostained images (D) are shown. N=3. Graph shows mean±S.D. (**E**) STMN2 undergoes phosphorylation early during stress. Calf intestinal phosphatase (CIP) treatment of cell lysates from stressed cells reverses stress-induced STMN2 mobility shift. Representative western blot is shown. (**F**) STMN2 phosphorylation sites. Serines in red were mutated to Alanines in STMN2-3A expression construct. (**G,H**) Reduced phosphorylation of STMN2 does not affect its distribution or stability. Representative immunostaining images (G) and western blot (H) are shown. Purple asterisk indicates endogenous STMN2 and green asterisk – GFP-tagged variants. Protein levels were quantified by densitometry. N=3. (**I,J**) STMN2 redistribution correlates with Golgi fragmentation early in stress. Representative images and quantification for SH-SY5Y cells (I) and representative images for human motor neurons (J) are shown. "None", "partial", and "intact" – STMN2 overlap with Golgi staining. SH-SY5Y cells were used except in J. Scale bars, 10 µm. Figure partially created in BioRender. Shelkovnikova, T. (2026) https://BioRender.com/zawd4u5.

Figure 3 STMN2 protein synthesis is maintained under acute stress with global translation repression. (**A,B**) Transient restoration of STMN2 protein level early during the recovery from arsenite stress. Representative western blot and protein quantification (A) and representative images for immunostaining (B) are shown. N=3. Scale bar, 10 µm. (**C**) Puro-PLA approach. (**D**) Ongoing STMN2 translation under acute stress, as revealed by puro-PLA analysis. Puro-PLA signals were quantified in an automated way on Opera Phenix/Harmony. N=6, n>3000 cells per condition. **p<0.01, Mann-Whitney *U* test. "Single ab", anti-STMN2 antibody alone was used. Scale bar, 25 µm. SH-SY5Y cells were used. Graphs show mean±S.D. Figure partially created in BioRender. Shelkovnikova, T. (2026) https://BioRender.com/734gwwq.

Figure 4 Stress granules contribute to STMN2 regulation under stress. (**A**) Integrated stress response and its modulation by small molecules. (**B,C**) eIF4A inhibition with small molecules leads to rapid and dramatic STMN2 depletion. Representative western blot (B) and quantification (C) are shown. Cells were treated with the indicated compounds for one hour. N=3; *p<0.05, **p<0.01, ***p<0.001, ****p<0.0001, one-way ANOVA with Dunnett's post-hoc test. (**D**) eIF4A inhibitors and phospho-eF2α dependent stressors induce stress

granule assembly. Representative images are shown. Scale bar, 10 μm. (**E**) STMN2 mRNA segregates into distinct clusters/foci in response to stress. Single-molecule RNA-FISH with a custom probe was used. Arrowheads point to the STMN2 mRNA clusters/foci. Scale bar, 25 μm. (**F**) STMN2 mRNA is significantly enriched in stress granules. Quantification and representative images are shown. Arrowheads point to G3BP1-positive foci – stress granules. Stress granules from 114 cells were included in the analysis. **p<0.01, ***p<0.001, ****p<0.0001, one-way ANOVA with Dunnett's post-hoc test. Scale bar, 10 μm. (**G**) STMN2 protein synthesis occurs outside of stress granules. Newly synthesised STMN2 protein molecules were visualised by puro-PLA and stress granules – by G3BP1 immunocytochemistry. 570 stress granules were included in the analysis from a representative experiment. Arrow indicates a stress granule with PLA signals on the surface. Scale bar 10 μm. (**H**) ISRIB and lipoamide interfere with stress granule assembly. Stress granule assembly was induced by $NaAsO_2$. Representative images and automated quantification are shown. N=3 (500-1000 cells analysed in each experiment). ***/$^{\#\#\#}$p<0.001, ****/$^{\#\#\#\#}$p<0.0001, two-way ANOVA. Scale bar 10 μm. (**I**) ISRIB and lipoamide attenuate STMN2 depletion during the recovery from stress. Cells were pre-treated with either ISRIB or lipoamide, which was replenished before the recovery from stress (continuous presence of the compound in the media). Representative western blot and quantification are shown. N=5; *p<0.05, **p<0.01, Mann-Whitney *U* tests. SH-SY5Y cells were used. Graphs show mean±S.D. Figure partially created in BioRender. Shelkovnikova, T. (2026) https://BioRender.com/n1yqn36.

Figure 5 Chronic stress leads to attenuated translation and STMN2 protein depletion. (**A**) Stress paradigms used in the study for SH-SY5Y cells and human motor neurons. (**B,C**) Chronic, but not repetitive, stress downregulates STMN2 protein. Representative western blot and quantification (B) and representative immunostaining images (C) are shown for SH-SY5Y cells. N=3; *p<0.05, Mann-Whitney *U* test. Scale bar 15 μm. (**D**) Chronic or repetitive stress do not cause visible changes in TDP-43 subcellular distribution or nuclear condensation. Representative images for SH-SY5Y cells are shown. Scale bar, 10 μm. (**E**) Chronic stress leads to reduction in global protein translation. Translation efficiency was measured by ribopuromycilation in SH-SY5Y cells after applying the chronic stress paradigm shown in A. Representative western blot is shown. (**F**) STMN2 has a short half-life and is more stable in postmitotic compared to proliferative neuronal cells, as demonstrated by cycloheximide (CHX) pulse-chase. Rocaglamide-A and sylvestrol were included as additional controls – translation inhibitors (30-min treatment). Representative western blots and protein level quantification by densitometry are shown. N=3. Graph shows mean±S.D. (**G**) Chronic stress causes Golgi apparatus fragmentation in human

motor neurons. Representative images and quantification are shown. Cells were analysed at the end of 48 hours as in A. (**H**) Chronic, but not repetitive, stress results in increased cell death in SH-SY5Y cultures. Cell viability was measured on Incucyte using a caspase-3/7 dye. Data were normalised to the 0-h time-point. N=3; ****p<0.0001, one-way ANOVA with Tukey's post-hoc test. Graph shows mean±S.E.M. (**I**) Chronic, but not repetitive, stress results in increased cell death in human motor neuron cultures. Cell viability was measured on Incucyte using a caspase-3/7 dye. Data were normalised to the 0-h time-point. N=4; ****p<0.0001, one-way ANOVA with Tukey's post-hoc test. Graph shows mean±S.E.M. Figure partially created in BioRender. Shelkovnikova, T. (2026) https://BioRender.com/ju6mqeg.

Figure 6 Pre-stress STMN2 protein level influences neuronal cell survival under stress. (**A**) Efficient siRNA-mediated STMN2 knockdown. Representative images and western blot are shown. N=4. Cells were analysed 24 h post-transfection. Scale bar, 10 µm. (**B**) STMN2 knockdown does not significantly affect cell proliferation or viability under basal conditions, but is associated with impaired proliferation and survival under stress. Cells were stressed with $NaAsO_2$ 24 hours post-transfection, washed and imaged during the recovery. N=3, ****p<0.0001, one-way ANOVA with Tukey's post-hoc test. (**C**) STMN2 overexpression using lentiviral delivery. Representative images and western blot are shown. N=2. Cells were analysed (with or without arsenite stress) 48 hours post-transduction with STMN2- or control protein (Cry2olig)-expressing lentivirus. Scale bar, 10 µm. (**D**) Moderate STMN2 upregulation does not significantly affect cell proliferation or viability under basal conditions but protects cells from apoptosis under stress. Cells transduced to express untagged STMN2 or control protein were monitored for 24 hours of recovery from $NaAsO_2$ stress. Cells were subjected to stress 48 hours post-transduction. N=4, ***p<0.001, one-way ANOVA with Tukey's post-hoc test. **(E)** Statin pre-treatment protects from stress-induced apoptosis. Cells were treated with pitavastatin for 16 hours, stressed with $NaAsO_2$, washed and imaged during the recovery period. N=3; **p<0.01, ****p<0.0001, one-way ANOVA with Dunnett's post-hoc test. Scale bar, 100 µm. SH-SY5Y cells were used. Graphs show mean±S.E.M.

Figure 7 STMN2 protein levels are sustained in non-TDP ALS. (**A,B**) STMN2 protein is significantly depleted in spinal motor neurons of sporadic ALS (sALS) patients. Representative images (A) and quantification (B) are shown. N=5; 153 and 96 individual motor neurons analysed for control and sALS, respectively. Arrowheads indicate motor neurons. **p<0.01, ****p<0.0001, Mann-Whitney *U* test. Scale bars, 100 µm. (**C**) STMN2

mRNA is downregulated in sALS motor neurons. STMN2 full-length mRNA was detected by BaseScope ISH using an exon 4/5-specific probe. Representative images are shown. Scale bars, 100 µm. (**D**) STMN2 protein level is sustained in non-TDP ALS subtypes. Representative images and quantification are shown. N=3, 2 and 3 for healthy controls, ALS-FUS and ALS-SOD1, respectively; 163, 84 and 208 individual motor neurons analysed for controls, ALS-FUS and ALS-SOD1, respectively. Arrowheads indicate motor neurons. Scale bars, 100 µm. Graphs show mean±S.D.

Figure 8 Compensatory upregulation of STMN2 mRNA in ALS. (**A**) STMN2 protein level is sustained in a physiological ALS-FUS cell model. Quantification for FUSΔNLS SH-SY5Y lines is shown. N=3. Graph shows mean±S.D. (**B**) STMN2 mRNA upregulation in ALS-FUS cell models. Refs.[27,64,65] (**C**) STMN2 pre-mRNA upregulation in a physiological ALS-FUS cell model. Quantification for FUSΔNLS SH-SY5Y lines is shown. *p=0.05, Mann-Whitney *U* test. N=3. Graph shows mean±S.D. (**D**) STMN2 mRNA is upregulated in the CNS areas of sporadic ALS patients with low pathology burden. Bulk RNA-seq datasets from the NYGC ALS consortium were used (~200 sporadic ALS patients and ALS-free controls). Plot shows: median (central line), 25th to 75th percentiles (box), and min to max values (whiskers). (**E**) STMN2 RNA analysis in ALS-TDP motor cortex using qRT-PCR. N=4 per group, Mann-Whitney *U* test. Graphs show mean±S.E.M. (**F**) Model: STMN2 regulation under stress and in ALS. Figure partially created in BioRender. Shelkovnikova, T. (2026) https://BioRender.com/ju6mqeg.

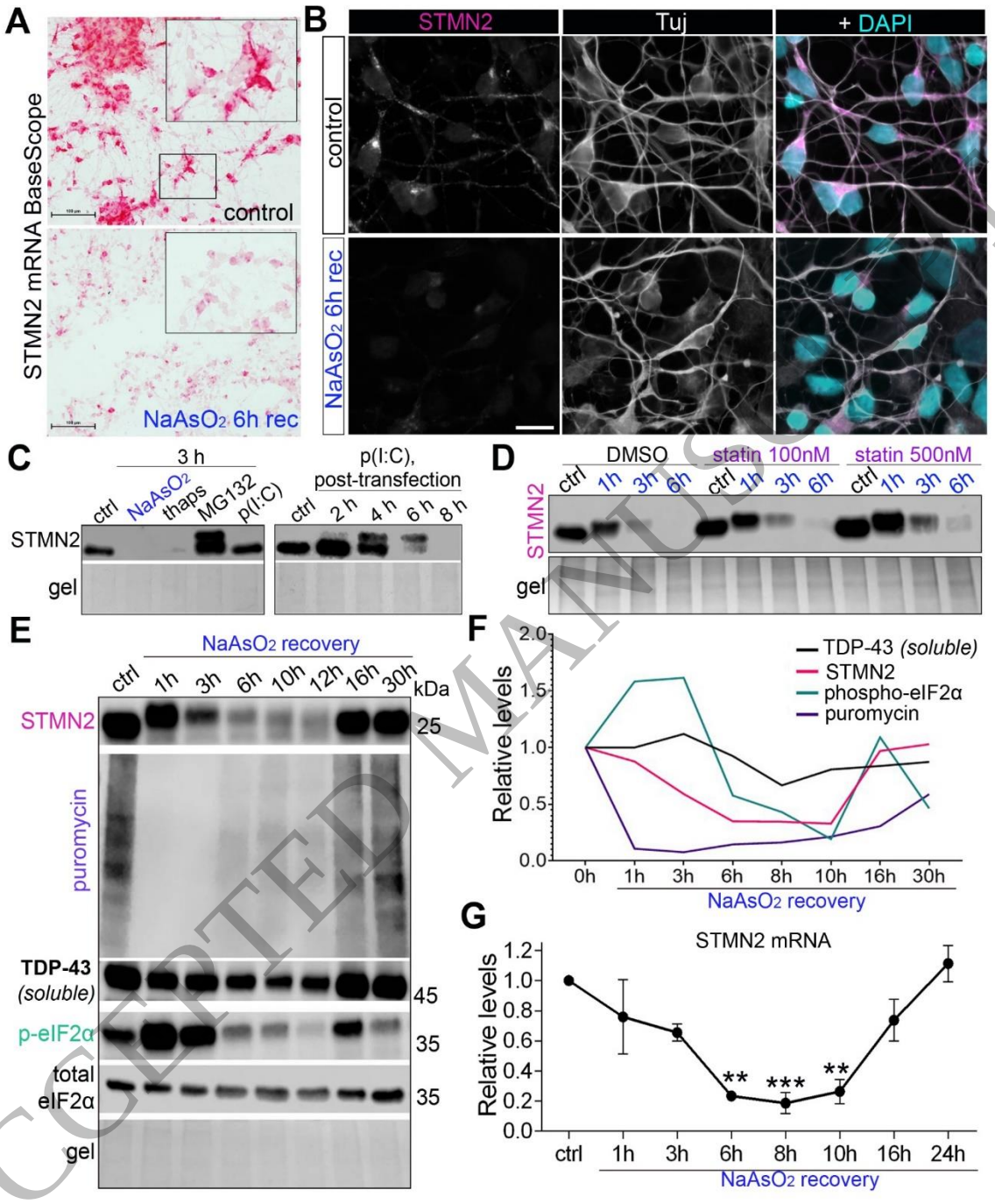

Figure 1
210x246 mm (x DPI)

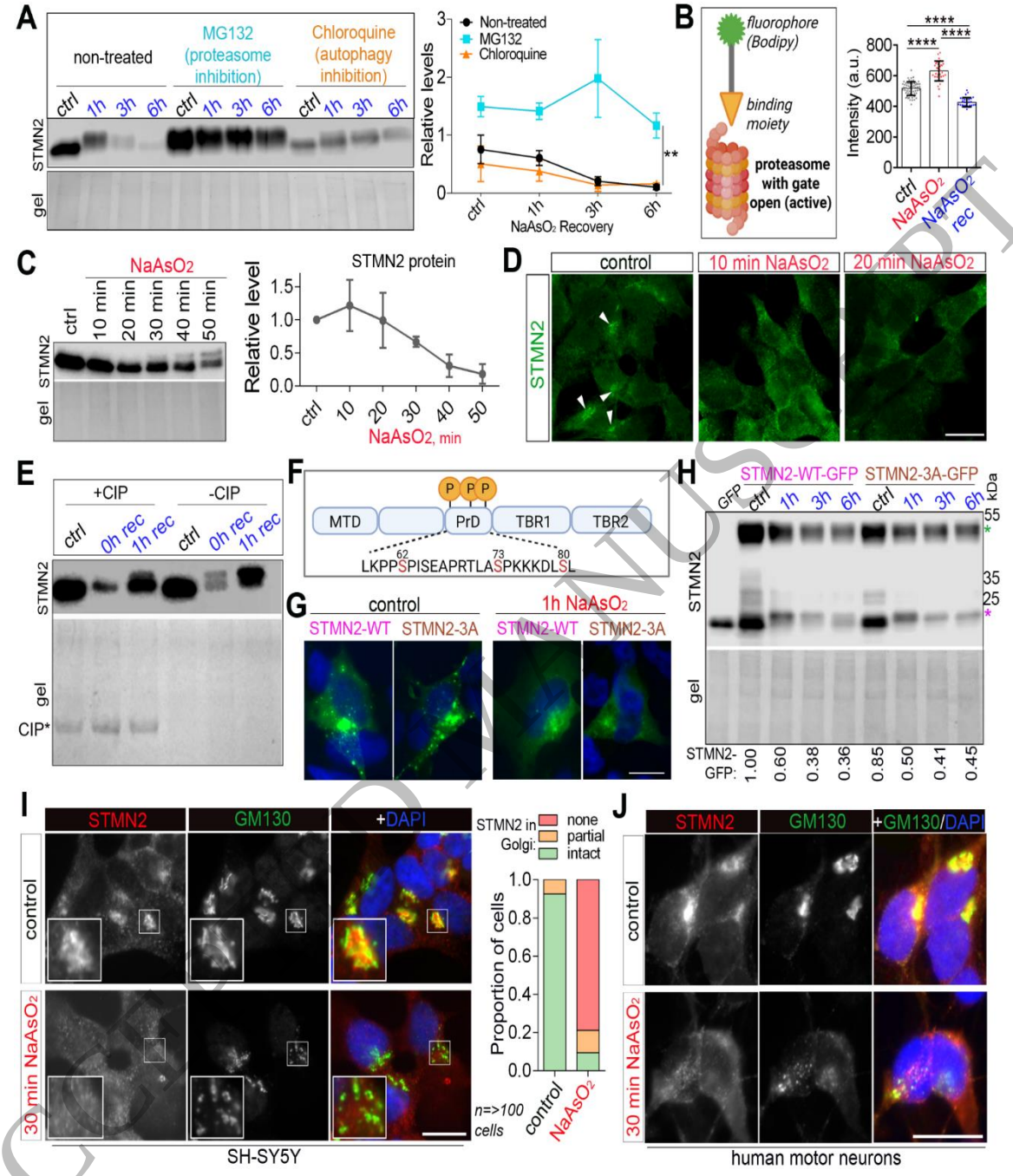

Figure 2
210x213 mm (x DPI)

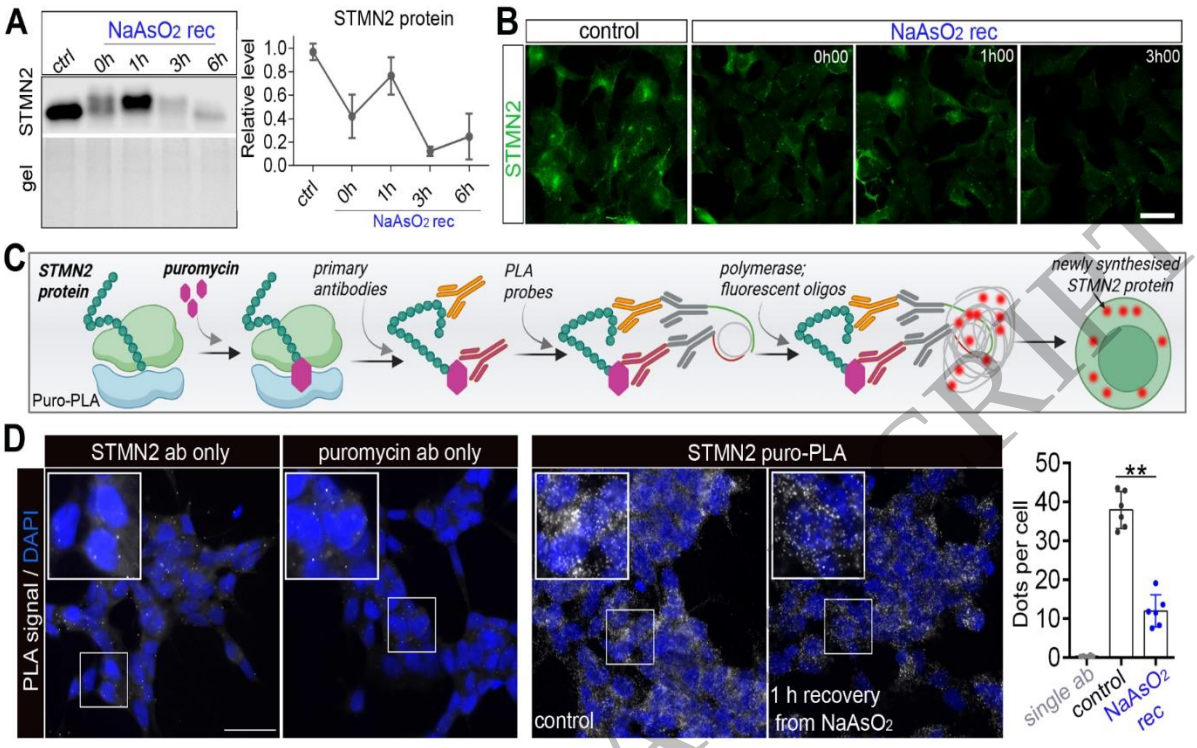

Figure 3
210x116 mm (x DPI)

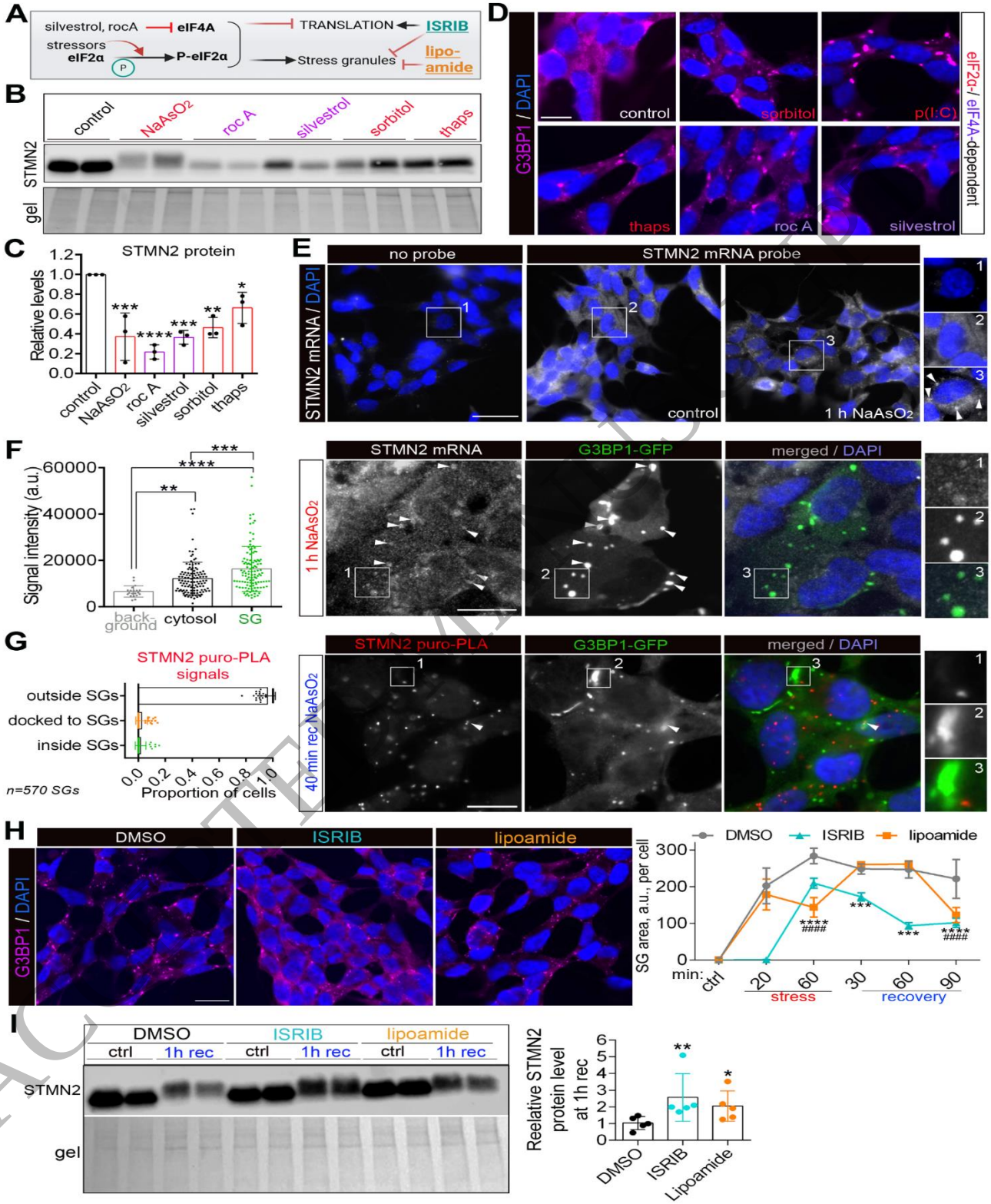

Figure 4
210x306 mm (x DPI)

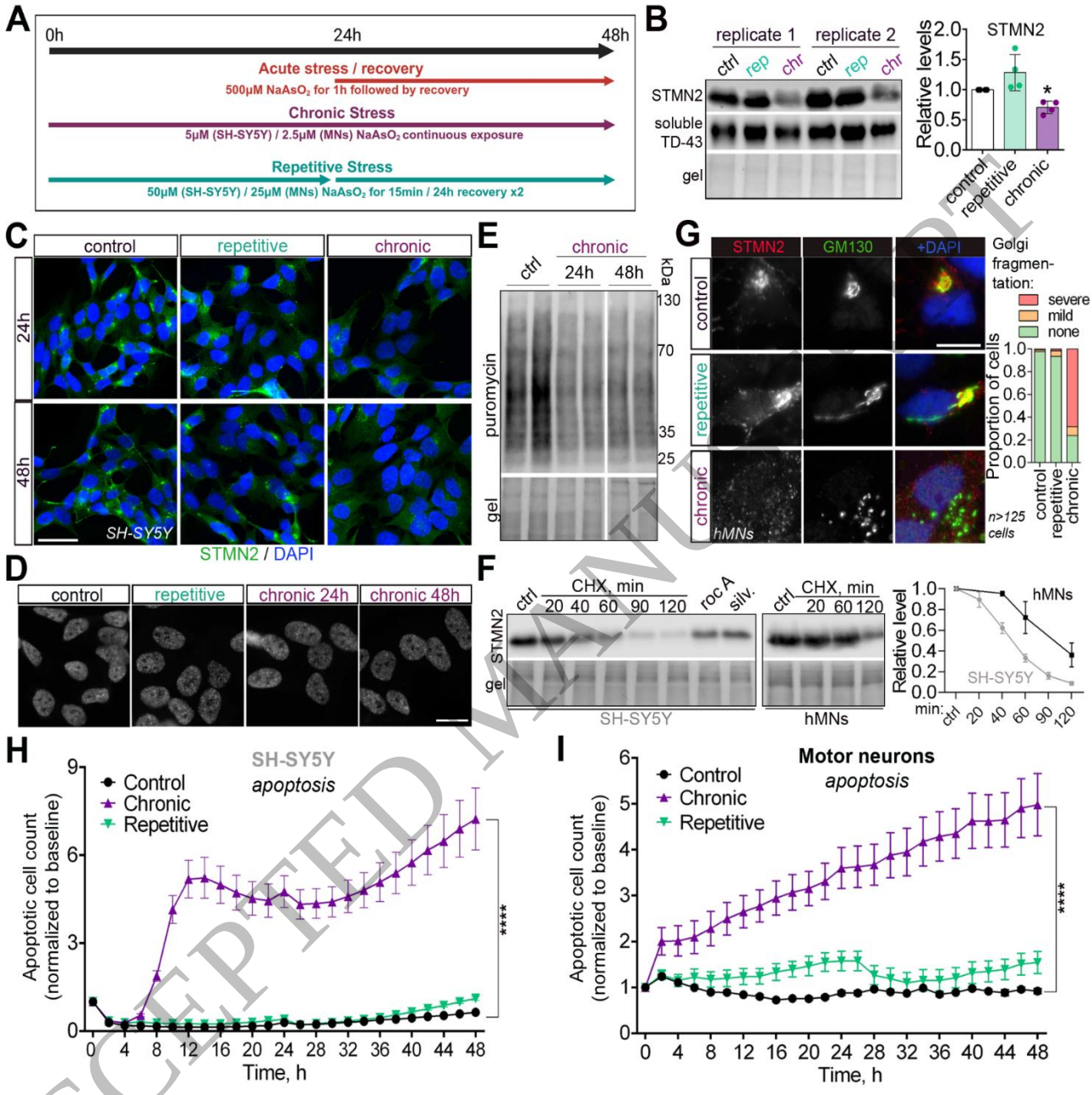

Figure 5
210x199 mm (x DPI)

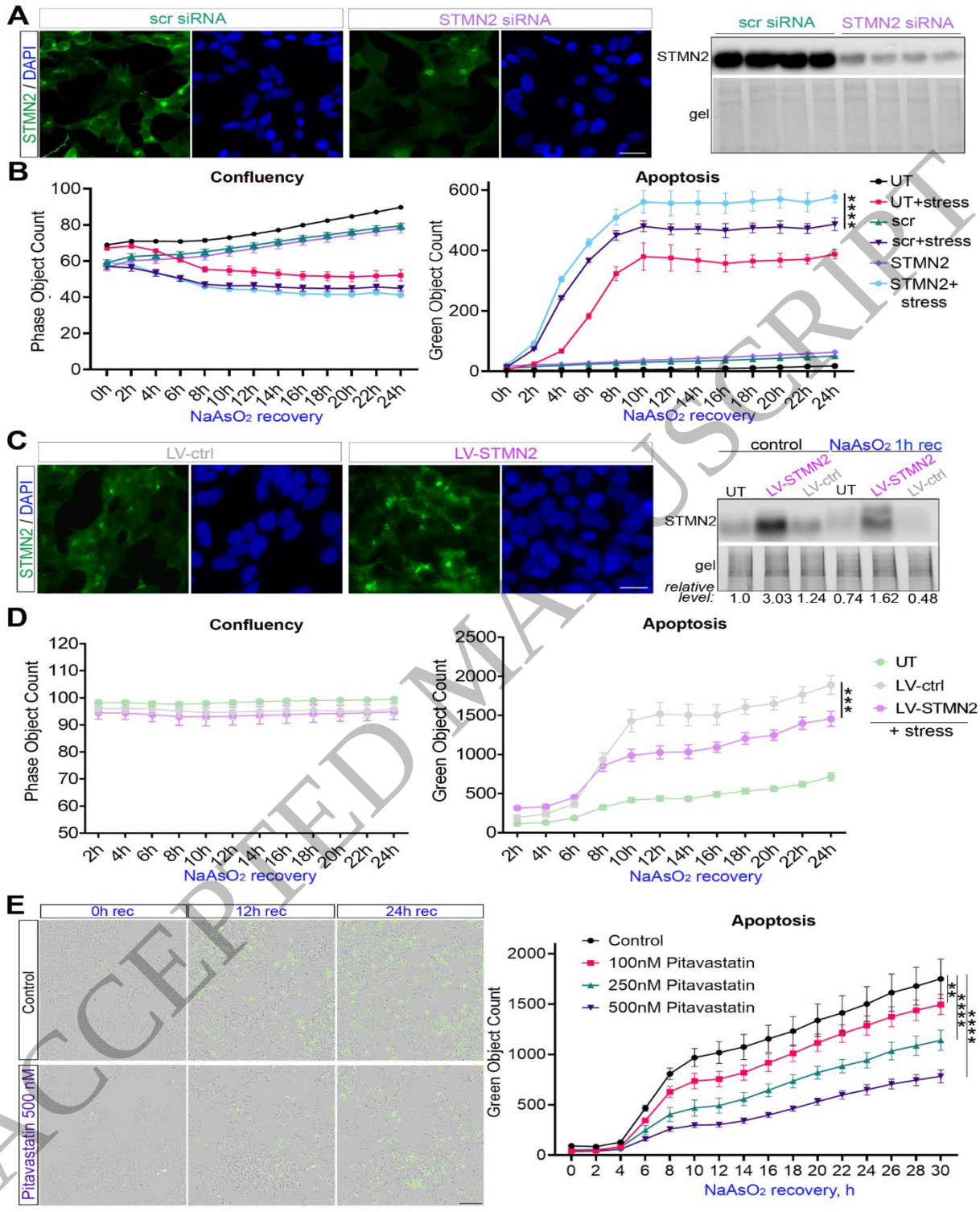

Figure 6
210x301 mm (x DPI)

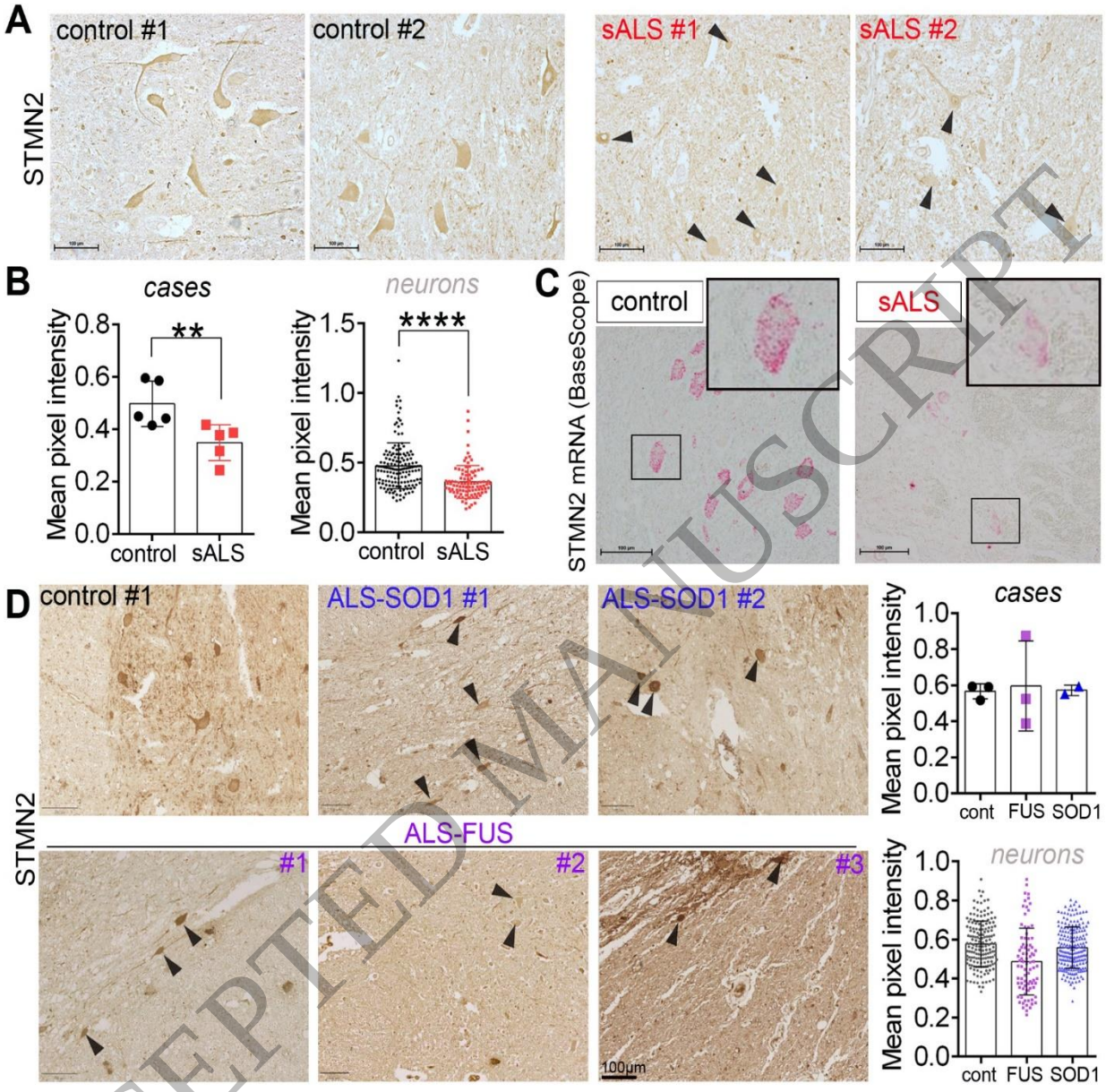

Figure 7
210x191 mm (x DPI)

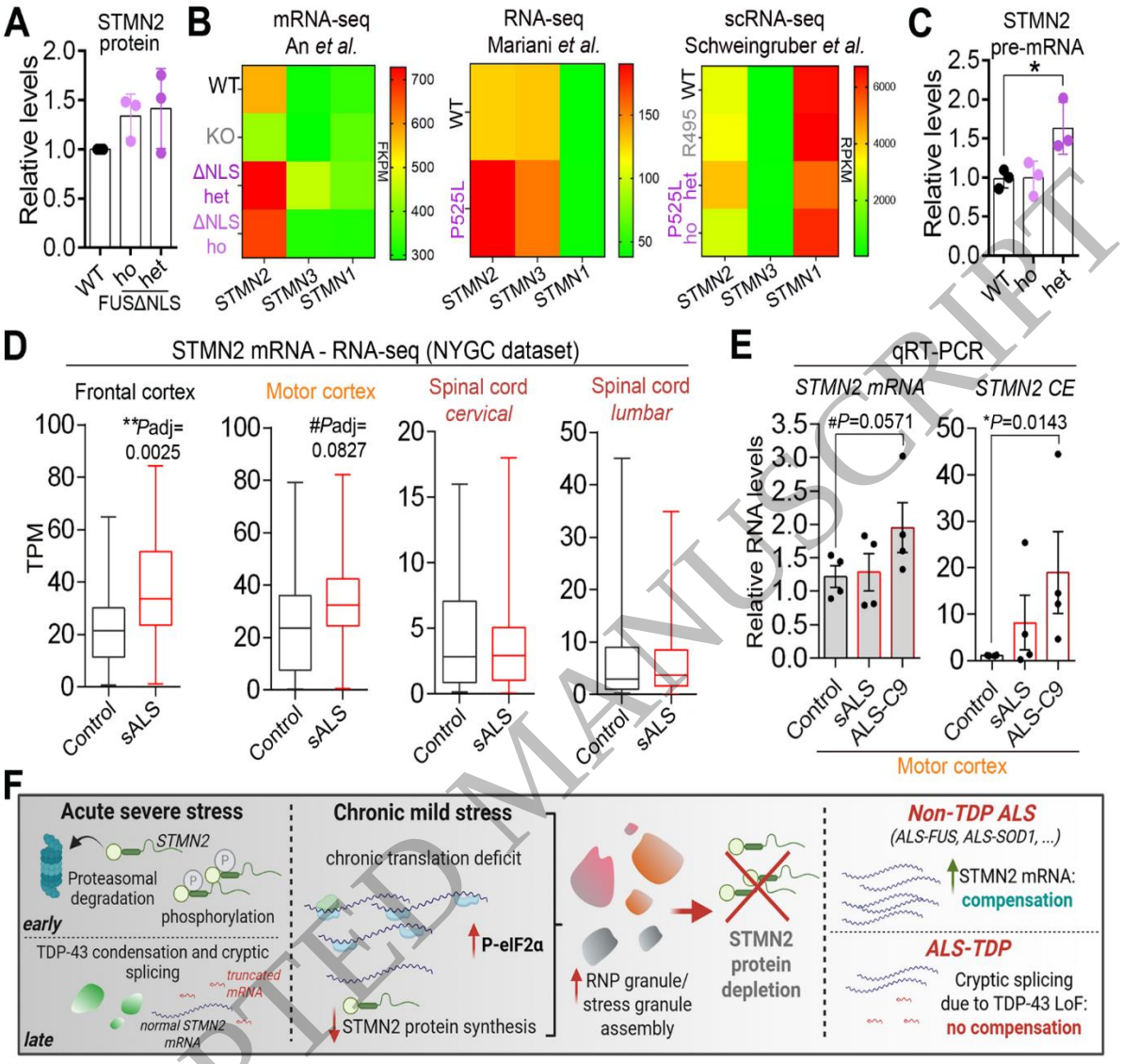

Figure 8
210x179 mm (x DPI)